Nanoscale

Accepted Manuscript

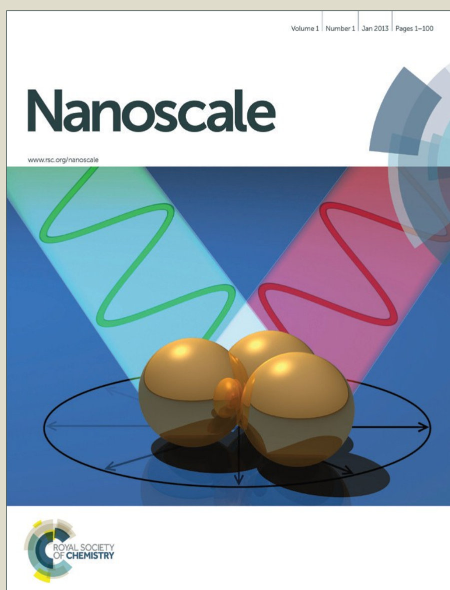

This is an *Accepted Manuscript*, which has been through the Royal Society of Chemistry peer review process and has been accepted for publication.

Accepted Manuscripts are published online shortly after acceptance, before technical editing, formatting and proof reading. Using this free service, authors can make their results available to the community, in citable form, before we publish the edited article. We will replace this *Accepted Manuscript* with the edited and formatted *Advance Article* as soon as it is available.

You can find more information about *Accepted Manuscripts* in the Information for Authors.

Please note that technical editing may introduce minor changes to the text and/or graphics, which may alter content. The journal's standard Terms & Conditions and the Ethical guidelines still apply. In no event shall the Royal Society of Chemistry be held responsible for any errors or omissions in this *Accepted Manuscript* or any consequences arising from the use of any information it contains.

ROYAL SOCIETY OF CHEMISTRY

www.rsc.org/nanoscale

Cracking-assisted Fabrication of Nanoscale Patterns for Micro/Nanotechnological Applications

Minseok Kim[1], Dong-Joo Kim[1], Dogyeong Ha[1], and Taesung Kim[1,2*]

[1]Department of Mechanical Engineering, Ulsan National Institute of Science and Technology (UNIST), 50 UNIST-gil, Eonyang-eup, Ulsan, 689-798, Republic of Korea

[2]Department of Biomedical Engineering, Ulsan National Institute of Science and Technology (UNIST), 50 UNIST-gil, Eonyang-eup, Ulsan, 689-798, Republic of Korea

[*]CORRESPONDENCE:

Taesung Kim
Department of Mechanical Engineering
Ulsan National Institute of Science and Technology (UNIST)
50 UNIST-gil, Eonyang-eup, Ulsan 689-798, Republic of Korea
E-mail:tskim@unist.ac.kr
Tel: +82-52-217-2313
Fax: +82-52-217-2409

Nanoscale Accepted Manuscript

Abstract

Cracks are frequently observed in daily life, but they are rarely welcomed and are considered a material failure mode. Interestingly, cracks cause critical problems in various micro/nanofabrication processes such as colloidal assembly, thin film deposition, and even standard photolithography because they are hard to avoid or control. However, increasing attention has been given recently to control and use of cracks as a facile, low-cost strategy for producing highly ordered nanopatterns. Specifically, cracking is the breakage of molecular bonds and occurs simultaneously over a large area, enabling fabrication of nanoscale patterns at both high resolution and high throughput, which are difficult to obtain simultaneously using conventional nanofabrication techniques. In this review, we discuss various cracking-assisted nanofabrication techniques, referred to as crack lithography, and summarize the fabrication principles, procedures, and characteristics of the crack patterns, such as their position, direction, and dimensions. First, we categorize crack lithography techniques into three technical development levels according to the directional freedom of the crack patterns: randomly oriented, unidirectional, or multidirectional. Then, we describe a wide range of novel practical devices fabricated by crack lithography, including bioassay platforms, nanofluidic devices, nanowire sensors, and even biomimetic mechanosensors.

Keywords: crack lithography, nanofabrication, nanopatterns and nanostructures, crack patterns, nanofluidic devices.

Nanoscale Accepted Manuscript

1. Introduction

Creating patterns and structures with dimensional sizes of 1–100 nm has played a crucial role in developing innovative nanotechnology that can precisely manipulate the motion and behavior of individual molecules[1]. Therefore, a facile but accurate nanofabrication method makes possible a variety of applications in both science and engineering fields, encompassing nanomaterials[2, 3], nanoelectronics[4], nanomechanics[5], nanobiotechnology[6], nanoenergy[7], and various nanodevices[8]. To date, substantial efforts have been made to develop reliable nanofabrication techniques, which can be categorized into conventional and unconventional ones.

1.1. Conventional nanofabrication techniques. First, electron-beam lithography (EBL, Fig. 1A)[9-11] is among the most precise methods of fabricating nanopatterns. EBL equipment emits high-voltage electrons (1–100 kV) to electron-sensitive or electron-resistive polymers (e.g. poly(methyl methacrylate)) to selectively remove unexposed or exposed resist. The patterning process of EBL is similar to that of photolithography; it consists of resist coating, exposure, and development processes but does not require masking structures during the exposure step because the EBL draws patterns directly using nanoscale e-beams with an automated scanning system. Similar to EBL, the focused ion beam (FIB)[12-14] technique uses sequential exposure of nanoscale ion beam spots that can physically damage a substrate by ion bombardment. Because the power density of the ion beam ($\sim 10^9$ W/cm^2)[15] is much higher than that of an e-beam (10^7 W/cm^2)[16], it can directly generate nanoscale grooved patterns on a hard substrate without the use of masking structures and resist deposition. Although EBL and FIB lithography can create nanopatterns at a high resolution of up to a few nanometers[17], direct writing by nanoscale beams limits the fabrication throughput, making it costly and time-consuming to produce large-scale nanopatterns. In addition, EBL and FIB lithography operate under high-vacuum conditions (typically 10^{-6}–10^{-10} Torr); therefore, it costs somewhat to set up and maintain facilities[9].

Nanoscale Accepted Manuscript

Second, the throughput limitation can be partially resolved by using nanoimprint lithography (NIL, Fig. 1B)[18-20], which replicates predefined nanopatterns on a rigid template by mechanically pressing conformal imprint resists. After the imprint resist is deformed, photoenergy or thermal energy is applied to harden the resist, and the master mold is released. In this manner, a number of nanopatterns can be duplicated repeatedly from an original master mold. Soft lithography[21] is a similar duplication method in which silicone elastomeric precursor solutions are thermally cured. NIL and soft lithography enable high-throughput nanofabrication. However, they can be cost-ineffective when a template mold is usable for only a limited number of replications, and new master molds must be produced by other expensive nanofabrication techniques.

Third, another common approach to producing nanopatterns is top-down or bottom-up surface and bulk micromachining techniques such as silicon (Si) etching[22, 23] and thin film deposition[24, 25] in conjunction with selective patterning of photoresists as masking layers *via* photolithography[26] (Fig. 1C). Standard photolithography by Si etching is used for fabricating two-dimensional (2-D) nanopatterns that have nanoscale heights but microscale widths and lengths, resulting in a low aspect (width to height) ratio[27, 28]. The bulk Si material is usually eliminated by dry etching (e.g., reactive ion etching, RIE)[22] or wet etching (e.g., using a potassium hydroxide solution)[29]. Thus, the critical dimension for nanopatterns (height) is controllable by adjusting the etching rate of the Si substrate. Two-dimensional nanopatterns are also fabricated by surface nanomachining (thin film deposition) with photolithography-based photoresist patterning for the sacrificial layer process (SLP)[28, 30]. The SLP is a representative bottom-up approach that uses sequential stacking of selectively patterned thin films. Photolithography by Si etching or thin film deposition is relatively simple and cost-efficient because it uses batch processing over a large-scale wafer, but the applications of the nanopatterns can be limited by their 2-D profile[28]; it is difficult to produce submicron line patterns, including one dimensional (1-D) nanowire and nanoscale spots, by photolithography-based micro-electro-mechanical system (MEMS) techniques.

Nanoscale Accepted Manuscript

1.2. Unconventional nanofabrication by cracking. As summarized in Fig. 1, conventional nanolithography methods such as EBL and FIB lithography have superior resolution but inferior fabrication throughput (Fig. 1A). Photolithography-based MEMS techniques, in contrast, show limited patterning resolutions of up to a micron in line width, but simultaneously produce massively parallelized patterns by batch fabrication (Fig. 1C). On the other hand, NIL and soft lithography exhibit intermediate levels of both resolution and throughput; however, they are essentially replication methods that rely on other nanofabrication techniques to duplicate original master molds (Fig. 1B). Thus, a nanofabrication technique that can produce patterns or structures with a high resolution and high throughput is urgently required.

Recently, designed material failures of thin films such as cracking[31-46], buckling (wrinkling)[47-53], and folding[54-56] have been introduced as time- and cost-efficient methods of creating nanopatterns. Although these morphological instabilities of thin films were considered as complex and chaotic phenomena, it was possible to generate well-organized nanopatterns by spatiotemporal engineering of the applied stresses and material properties. In particular, cracking-assisted nanofabrication, called crack lithography in this work, seems to be the most promising alternative because it can simultaneously produce nanopatterns over a large-scale substrate (high throughput)[3, 35] and accurately control the feature size up to a few nanometers (high resolution)[35, 57]. For instance, as shown in Fig 1D, nanoscale cracking produces various propagating trajectories (patterns) such as oscillating, straight and stitch-like lines over a large-scale wafer at the same time. The cracks can either penetrate the substrates or be localized within thin films without a wide range of material choices, including popular semiconductor materials such as Si, SiO_2, and metals. In addition, cracking dimensions such as widths and depths seem to be comparable to the state-of-the-art resolution of conventional nanofabrication with dramatically reduced cost and time consumption without use of complex and expensive facilities.

Nanoscale Accepted Manuscript

In 1998, the first comprehensive attempt was made to utilize intentional generation of cracks as well-defined nanostructures by combinatorial material choices between thin films and substrates during chemical vapor deposition (CVD)[57]. The next wave in cracking-assisted nanopatterns was in practical applications such as nanowires (2004)[42, 58], cellular patterning (2005)[33], and nanofluidic devices (2007)[36]. Then, in 2012, crack lithography enabled high throughput nanofabrication at a wafer level by batch processing[35], which was typically expensive and time consuming using conventional nanolithography techniques. In 2015, the throughput and controllability of crack lithography were fairly enhanced by controlling dimensions, directions, and propagating kinetics of nanoscale cracks with a spatiotemporal engineering of material properties and applied tensile stresses[38, 59]. Hence, crack lithography techniques became increasingly advanced in terms of not only their patterning capability such as resolution and throughput, but also extension of application fields.

In this review, we survey various crack lithography techniques for producing nanopatterns and categorize them into three technical development levels based on the controllability of the nanopatterning directions of the cracks: randomly oriented, unidirectional, or multidirectional. In addition, we review a wide range of applications of the nanopatterns produced by crack lithography, including biomolecular and cellular patterning, nanofluidic devices for mass-transport control, nanowire-integrated gas sensors, and even biomimetic multifunctional mechanosensors. Although several reviews on cracking-based patterning were reported previously, they considered only the fabrication of nanofluidic devices and biological applications[60, 61]. To the best of our knowledge, this review is the first to comprehensively investigate crack-assisted lithography techniques considering not only their nanopatterning capabilities but also a wide range of applications.

2. Fundamentals in cracking

Nanoscale Accepted Manuscript

In principle, cracking is physical breakdown of the interaction (bonding) energy between adjacent atoms without complete separation of parts (fracture); it occurs when the applied tensile stress exceeds the ability of a material containing a crack to resist fracture, called the fracture toughness (also called the critical stress intensity factor, $\boldsymbol{K}_c$ (Pa·m$^{0.5}$))[62]. The stress intensity factor ($\boldsymbol{K}$), which has the same physical unit as $\boldsymbol{K}_c$ (stress times the root of distance), is used for predicting how much a nominal tensile stress caused by external loads or residual effects is intensified near the tip of a crack. The magnitude of $\boldsymbol{K}$ is an extensive material property that depends on the size, position and shape of cracks, and the magnitude and applied rate of loads on the material. In theory, there are three pure fracture modes depending on the direction of applied loads: Mode I–opening (tensile), Mode II–sliding (in-plane shear), and Mode III–tearing (out-of-plane shear). The linearly independent cracking modes often appear together resulting in complex cracking phenomena with different magnitudes of $\boldsymbol{K}_c$ and $\boldsymbol{K}$ according to the fracture modes. However, especially for thin film and substrate systems, pure Mode I is the most typical case, implying that the fracture toughness and stress intensity factor of Mode I ($\boldsymbol{K}_{Ic}$ and $\boldsymbol{K}_I$) are the most important factors determining whether a crack begins to grow. That is, a crack propagates when $\boldsymbol{K}_I \geq \boldsymbol{K}_{Ic}$ and remains unchanged when $\boldsymbol{K}_I < \boldsymbol{K}_{Ic}$, which seems to be predictable and controllable by accurate engineering of loading and material conditions.

Fig. 2 is imaginary cracking phenomena in a thin film, having a specific thickness (t_1), Young's modulus (E_1), and fracture toughness ($\boldsymbol{K}_{c,1}$), on a rigid substrate to show the engineering parameters for crack control. For example, a thin film and substrate system can often be exposed to various external forces during fabrication and treatment of the film, including electrical[63], optical[64], thermal[65], and even mechanical forces[66]. Because of the interaction between the materials (films and substrates) under the applied forces, an axial or isotropic tensile stress/strain can be induced in the film and amplified locally at sharp tip points such as notched microstructures. Because the nominal tensile stress field is concentrated around the notch, crack initiation at the

Nanoscale Accepted Manuscript

notched position is favorable, and the crack then propagates along the maximal stress field. During propagation, the crack can encounter another region that has different material properties (t_2, E_2, and $\boldsymbol{K}_{c,2}$). At the junction point, the crack can be terminated, redirected, or advanced with a different propagation velocity, depending on the local material properties of the new region. In addition, the crystallographic orientation of the substrate often affects the propagation direction of cracks, which can advance preferentially along the weakest bonding orientation. Consequently, these key factors, including the stress source, stress concentration effect, and material properties of the substrate and film, should be carefully engineered to control cracks so as to create nanopatterns at high resolution and high throughput.

3. Randomly oriented crack patterns

Fractal-like random structures created by cracking are observed frequently in various thin film and colloidal processes because high residual tensile stresses can be generated spontaneously by baking, drying, and deposition. In this section, we review randomly oriented crack patterns generated by solvent evaporation (drying) of self-assembled colloidal structures and by thin film CVD to understand the fundamental mechanisms of nanoscale cracking phenomena, which seems to be essential for advancing toward exquisitely controlled crack patterns.

3.1. Drying-mediated random cracks. Fig. 3A shows randomly oriented crack patterns in a self-assembled monolayer of uniformly sized polystyrene microspheres (d = 3.4 μm)[67]. For the cracking analysis, a close-packed, monolayered colloidal film was prepared with a relatively large grain size (10^5–10^6 spheres) by sandwiching the polystyrene microspheres between glass slabs, followed by a slow drying process. In the first step, localized defects such as vacancies and grain boundaries nucleated slowly without cracking because the stress concentration was insufficient to initiate cracks. After sharp tips formed at defective points, cracks were initiated and then propagated rapidly and linearly, as shown in both empirical (top images) and numerical (bottom images) results

Nanoscale Accepted Manuscript

in the initial images in Fig. 3A. The rapid linear propagation was attributed to the stress concentration effects at the sharp tips of the defects. During propagation, some cracks merged with adjacent cracks by changing their propagation directions or branched into multiple but smaller cracks. In the final stage, crack propagation slowed and become nonlinear because the tensile stress caused by dehydration of the microspheres was non-uniform, resulting in the formation of complex fractal-like random cracks. After drying was complete, the average diameter of the polystyrene spheres was reduced from 3.4 to 2.7 μm (approximately 20%), and all the cracks were completely terminated.

Rao et al. reported similar randomly oriented crack patterns during a drying process (25 °C, 5 min) of spin-coated colloidal solutions containing acrylic nanoparticles (d = 40–80 nm) on a glass substrate[68]. The drying-mediated cracks showed different dimensions and densities according to the thickness of the coating layer[69]. For example, as the film thickness increased from 0.6 to 9 μm, the crack width increased gradually, but the number of cracks was reduced (Fig. 3B). In addition, the material properties of the contained colloidal particles, such as the size, shape, and Young's modulus, greatly affected the cracking phenomena.

The drying process can induce not only a tensile stress but also a twisting stress field, which creates a spiral cracking pathway (Fig. 3C)[32]. *Leung et al*. dried a dilute aqueous suspension of a precipitate such as nickel phosphate ($Ni_3(PO_4)_2$) in a Petri dish. As the suspension dried, it solidified and then divided into a number of small pieces. After it splintered, further continuous drying created a spiral crack in a precipitate fragment that gradually became detached from the Petri dish from the outside to the inside because of humidity gradients along not only the normal but also the radial direction. That is, drying proceeded from the top and lateral surfaces to the bottom and central part. This gradual and circular detachment of the precipitate fragment from the substrate induced a twisting stress field and created the spiral crack patterns; both experiments and numerical simulations revealed the same tendency (Fig. 3C). Interestingly, similar cracking phenomena

Nanoscale Accepted Manuscript

occurred in other aqueous precipitates such as ferric ferrocyanide ($Fe_4[Fe(CN)_6]_3$) and ferric hydroxide ($Fe(OH)_3$), although the profile and size of the spiral cracks varied depending on the fragment size, solidified film thickness, and precipitate type.

3.2. CVD-based random cracks. Randomly oriented cracks were also found during various CVD processes, which can naturally give rise to residual tensile stresses originating primarily from the mismatch in thermal expansion coefficients between the substrate and deposited thin films. In contrast to the drying-mediated stress, the residual stresses were more uniform (isotropic and homogeneous) throughout a large-scale material, but the crystallinity of the foundation substrate (e.g., a Si wafer) greatly affected the crack patterns. *Gorokhov et al*. first comprehensively investigated cracking phenomena in various CVD processes as a novel cracking-assisted nanofabrication concept[57]. For example, a glassy, brittle layer such as a Si oxide (SiO_2) or Si nitride (Si_3N_4) film was deposited on various substrates having different crystallographic orientations. As shown in Fig. 4A-i, a SiO_2 film was deposited on a (111)-oriented substrate using low-pressure CVD (LPCVD) at a relatively low deposition temperature (T_d = 100 °C) and exhibited linear propagation of cracks that tended to be aligned in the <112> direction. Fig. 4A-ii shows periodically oscillating crack patterns produced by 600 nm CVD of a Si_3N_4 film on a (100)-oriented Si substrate at T_d = 750 °C. The propagation direction of the oscillating crack was determined by the formation of a plastic deformation zone in the substrate, which caused crack propagation oriented in the <110> direction. Interestingly, cracks in the Si_3N_4 thin film penetrated deep into a substrate when the residual stress was high enough to break the bonding energy of the substrate. This implies that the crack directions and dimensions can depend strongly on the substrate properties. For example, Fig. 4A-iii shows crack patterns in the surface of the (001)-oriented Si substrate after a Si_3N_4 film produced by 500 nm CVD at T_d = 700 °C was peeled off. However, the effect of the crystallographic orientation of the substrate can be suppressed by positioning an amorphous interlayer as a damping layer between the thin film and substrate. The damping layer

Nanoscale Accepted Manuscript

generally possesses higher elastic and ductile characteristics (high fracture toughness) than the brittle thin film, so elastic and/or plastic deformation of the damper layer consumes the shear energy originating from crack propagation in the thin film[35, 57]. Fig. 4A-iv shows orientation-free cracks in a SiO_2 film (450 nm thick, T_d = 650 °C) on a (111)-oriented germanium (Ge) substrate with a viscous interlayer of germanium oxide (GeO_2). Notably, the crack patterns were totally random without preferential propagation directions because the interlayer prevented penetration of the cracks into the crystallized substrate. Thus, no plastic deformation zone was observed in the substrate, as confirmed by X-ray topography and transmission electron microscopy images.

Without employing an interlayer, *Luke et al.* and other researchers minimized the crystallographic effects by surrounding a cracking area with open trenches (etched Si patterns) in which crack propagation could not occur, as shown in Fig. 4B[70, 71]. Therefore, cracks initiated at random positions were terminated at the crack-free trenches, which kept the cracks from spreading or escaping to inside or outside of the crack-free regions. Cracks in the Si_3N_4 film typically penetrated the substrate owing to the high residual stress (Fig. 4A-iii); thus, a simple grooved trench was insufficient to stably block the propagating cracks. To increase the propagation resistance, *Luke et al.* fabricated multiple (up to five) trenches in series and successfully terminated propagating cracks at the crack-free trenches.

The substantial randomness of the cracks found in both colloidal drying and thin film CVD processes arises from complex interrelations among the applied tensile stresses, the properties of the thin film (or colloid), the crystallographic orientation of the substrate, and even thermodynamic conditions such as the temperature and humidity. In fact, randomly oriented cracks are not suitable for use directly as an accurate nanofabrication method; however, systematic characterization of the crack patterns introduced in this section provides several important suggestions regarding the fundamental principles of nanoscale cracking phenomena. First, randomly distributed sharp tips in initial defects caused crack initiation at random positions. Thus, the employment of pre-engineered

Nanoscale Accepted Manuscript

sharp tips (notches) to concentrate the nominal tensile stresses would be advantageous for controlling crack initiation at desired positions. Second, the crystallographic orientation of the substrate greatly influenced the crack patterns, so it can be applied to guide the propagation direction. In particular, the substrate choice in CVD was important because cracks in thin films often penetrate deep into the substrate. Third, locally engineered material properties of the thin films or substrates can be used to localize crack patterns in specific regions by preventing unwanted generation of cracks in other regions (crack-free regions). Finally, a tensile stress applied for cracking should be carefully controlled because crack patterns were directly affected by the direction, magnitude, and application rate of the tensile stress. Given a comprehensive understanding of cracking phenomena, we would advance one step toward controlling cracks for accurate nanofabrication.

4. Unidirectional crack patterns

Randomly oriented cracks are initiated everywhere and then propagate without any preference for alignment with particular directions. This is because the intensity and directionality of the applied tensile stresses could not be controlled at specific positions and toward specific directions. For this reason, applications of randomly oriented crack patterns focused primarily on simple modification of surface properties and functionalities by opening new surface areas[41]. In this and the next sections, we introduce unidirectional and multidirectional crack patterns that can be aligned with particular single or multiple directions by precise control of the applied tensile stresses to create crack patterns at predetermined positions with controllable geometries.

4.1. Control of crack position by notched microstructure. The residual tensile stress generated during CVD of thin films (e.g., SiO_2 and Si_3N_4) is essentially homogeneous and isotropic, so a mechanism to locally amplify the nominal tensile stress was necessary to control the cracking positions and directions. For this purpose, many researchers employed stress-concentrating

Nanoscale Accepted Manuscript

microstructures such as notches and intentional defects, and created unidirectional crack patterns at predetermined positions[40, 72]. For example, *Mani and Saif* reported unidirectional crack patterns in a deposited SiO_2 thin film using prefabricated deep, narrow microscale trench structure (Fig. 5A)[72]. The trench structure was patterned by deep reactive ion etching (DRIE) on a Si substrate, followed by plasma-enhanced CVD (PECVD; 4 μm thick, T_d = 250 °C) of an oxide layer for non-conformal coverage of the top surface of the trenches. That is, the top surface of the trench was covered perfectly by the oxide layer. The inside of the trench, however, had unfilled voids with triangular cross-sectional profiles, because the SiO_2 deposition rate was maximum on the top surface and gradually decreased along the penetration depth of the trench. After an annealing process, a residual tensile stress was applied by a condensation reaction that caused volumetric shrinkage of the thin film, which was locally amplified at the sharp tip of the void[73]. In this way, a unidirectional crack pattern was created at the predetermined slender void and then propagated vertically as straight cracks, as shown in the scanning electron microscopy (SEM) images in Fig. 5A.

Similarly, *Alaca et al.* and other researchers developed other unidirectional crack patterns using prefabricated triangular notch structures for local concentration of the normal tensile stress at the sharp tip[40, 41, 74]. In fact, the stress-concentrating effects at sharp triangular notches were well-known in classical fracture mechanics[75, 76] but were rarely applied in microfabrication processes to control cracking phenomena until research was reported. Fig. 5B shows crack patterns in a deposited SiO_2 layer on a Si substrate; cracks were initiated at the notched positions and terminated at the open boundaries[41, 74]. To demonstrate the high-throughput capability of crack lithography, *Alaca et al.* prefabricated massively parallelized arrays of notches with a uniform spacing (50 μm) and line patterns using a 10 μm DRIE process. After the stress-modulating structures in the Si substrate were patterned, a 5–10-μm-thick SiO_2 film was deposited on the substrate using PECVD; then a heat treatment (400 °C for 20 min) was applied under a nitrogen atmosphere. The heat treatment was applied to generate residual tensile stress using thermal coefficient mismatch of the

Nanoscale Accepted Manuscript

Si substrate and SiO_2 film, which is also the same principle used for the CVD-based cracks described above.

Consequently, the sharp tips at the triangular notches controlled the positions of crack initiation by locally concentrating the nominal tensile stress, and the initiated cracks propagated linearly because of the homogeneity of the tensile stress and thin film. A high power density was used for the DRIE process to fabricate the sharp corners at the notches and open boundaries[41, 77], which was important for successfully controlling crack initiation and termination. In addition, *Xia et al.* evaluated the crack patterns in different notch-to-notch spaces because two approaching parallel cracks were attracted to each other, resulting in failures in the production of straight linear cracks[78, 79]. A minimum notch-to-notch space of 30 μm was chosen to guarantee linear crack propagation, although the specific value seems to depend on the CVD conditions.

4.2. Directional control by uniaxial tensile stress/strain. In contrast to spontaneous generation of residual tensile stress, uniaxial tensile stresses were directly applied using temperature gradients[37] and mechanical strains[33, 43, 80]. For example, *Yuse and Sano* fabricated unidirectional crack patterns on a quenched glass specimen along the maximal temperature stress field by placing the sample between hot and cold reservoirs (Fig. 6A)[37]. First of all, a small notch was prefabricated in the center and bottom of the long glass specimen to induce crack initiation at the predetermined notch point. Next, the glass specimen was heated for a few minutes to reach an equilibrium temperature with the hot reservoir and then gradually dipped into the cold reservoir using a linear motor holding the glass plate. Interestingly, the crack patterns were aligned in the temperature gradient direction and had various propagation profiles such as straight, oscillating, and nonlinear, depending on the intensity of the thermal stress. That is, the temperature difference between the hot and cold reservoirs (spatial gradient) and the temperature descending speed (temporal gradient) determined the intensity of the thermal stress.

Nanoscale Accepted Manuscript

In details, unidirectional straight crack patterns were created at temperature differences between 50 and 100 °C with a 50 $mm \cdot s^{-1}$ sample descent speed (Fig. 6A-i), whereas nonlinear, randomly bifurcated cracks were generated at temperature differences greater than 250 °C with the same descent speed (Fig. 6A-iii). In intermediate conditions, the crack patterns became quasilinear (unidirectional with oscillating curves, Fig. 6A-ii). The wavelength and amplitude of the oscillating curves were also controllable by adjusting the temperature difference and descent speed, which directly determined the spatiotemporal temperature gradient. Oscillating curves were generated because extra energy was generated at higher temperature differences and slower descent speeds than those that created linear cracks. In other word, the extra propagation energy and time gave the crack tip sufficient opportunity to communicate with the lateral boundaries of the glass specimen, so the crack patterns developed gradually from linear to mildly sinusoidal and then saturated oscillating, eventually becoming totally nonlinear, with increasing temperature difference. In addition, the critical transition conditions of the crack patterns were also influenced by the thicknesses and width of the glass plate.

A relatively simple but high-throughput mechanism for applying uniaxial tensile stress was demonstrated by controlling the strain rates of a thin brittle film deposited on an elastomeric polydimethylsiloxane (PDMS) substrate[33, 36, 43]. For example, *Zhu et al.* produced unidirectional crack patterns in a thin film by mechanically stretching a PDMS substrate using a high-precision jig[33]. The strain rate was applied using mechanical stretching, which can induce elastic deformation of the PDMS underlayer but create permanent deformation (cracks) in the brittle film on top. That is, the elastomer substrate has a higher fracture energy (460 ± 50 $J \cdot m^{-2}$ for PDMS)[81] than the brittle film because of its ductile, rubbery nature. Subsequently, a number of unidirectional crack patterns were fabricated in the thin film layer aligned perpendicular to the axial tensile strain direction[33, 36]. In addition, the dimensions and density of the unidirectional crack patterns were regulated by adjusting the magnitude and application rate of the strain.

Nanoscale Accepted Manuscript

More recently, the same group upgraded the strain-controlled cracking mechanism by combining it with triangular notch structures to more accurately control the crack position and density[43]. Fig. 6B shows the notch-guided unidirectional cracks patterns in an oxidized layer on the PDMS surface. The cracks in the oxide-PDMS system were controlled by adjusting the strain rate, deposited film thickness, and notch configuration. In particular, the design of the prefabricated notches greatly influenced the quality (yield rate) of the crack patterns; three notch structure configurations were tested: paired, unpaired, and alternating notches. When paired notches were used, the counter-facing cracks that were initiated individually at each notched point were occasionally misaligned. The unpaired notches also exhibited misalignment issues because the cracks were occasionally initiated from the open boundary without notches and merged with a counter-crack extending from the notched side. In contrast, the alternating notches showed far fewer alignment issues, producing linear crack arrays with a high production yield (Fig. 6B). One of the greatest advantages of the strain-controlled cracking mechanism is the simple fabrication process (stretching) using inexpensive equipment such as a strain-controlling element (e.g.., a linear motor). In addition, the mechanism can be applicable to various thin film materials including metals[43, 82], polymers[81], and even monolayered biomolecules[33] or nanoparticles[83], as long as the films can be uniformly coated on the flexible substrate.

5. Multidirectional crack patterns

5.1. Strain-controlled bidirectional cracks. Uniaxial strain-controlled cracks can be directly expanded to multidirectional ones by adding a strain-control unit for additional directions, although the directional freedom for cracking seems to be limited to a few directions owing to the complexity of the equipment required for large numbers of strain directions. *Kim et al.* deposited a relatively brittle, hard-PDMS (h-PDMS)[84, 85] thin film on a regular PDMS substrate and applied biaxial strains to the h-PDMS and PDMS composite to fabricate bidirectional crack patterns[44]. As shown

Nanoscale Accepted Manuscript

in Fig. 7, bidirectional crack patterns appeared in the h-PDMS film throughout all the rows and columns, guided by a diamond-shaped notch structure having four sharp tips. Interestingly, the cracks in the h-PDMS film could not penetrate the PDMS substrate and stopped at the interface between h-PDMS and PDMS. This result was attributed to the fact that h-PDMS and PDMS have comparable Young's modulus (9.2 and 3.7 MPa, respectively) but very different fracture energies (12.9 and 460 $J \cdot m^{-2}$, respectively)[84]. Thus, the height of the cracks can be controlled accurately by simply regulating the spin-coating parameters that determine the h-PDMS thickness. Generally, the thickness of previous thin films, such as oxidized PDMS or metal layers, on the PDMS substrate were unable to produce crack patterns larger than a micron, but h-PDMS is fabricated using a spin-coating method that can produce h-PDMS layers up to the microscale. Therefore, the crack patterns in the h-PDMS were relatively large, but their dimensions were recovered to the nanoscale by eliminating the applied strain because of the elasticity of the PDMS substrate.

5.2. CVD-based multidirectional cracks. CVD-based fabrication of uniaxial crack patterns can also be expanded to multidirectional cracks. *Nam et al.* fabricated various crack patterns in a Si_3N_4 film by LPCVD requiring high temperatures (T_d = 800 °C)[35], which can cause high residual stresses owing to the large thermal expansion mismatch between the film and substrate materials[73, 74]. As in the CVD-based cracking mechanism described above, they prefabricated stress-modulating microstructures such as notches and open boundaries in a Si wafer using the DRIE process to control crack initiation and termination at desired positions. The cracks in a Si_3N_4 film exhibited linear oscillating propagation with a tendency to be aligned in the <110> direction (Fig. 8A-i), and the oscillation curve was suppressed by inserting a SiO_2 interlayer that prevented penetration of the cracks into the Si substrate (Fig. 8A-ii), which is consistent with the results in Fig. 4A. Typically, it was not easy to terminate propagating cracks in a Si_3N_4 layer using simple single-layered trench structures (open boundaries) because the cracks in the Si_3N_4 film penetrated deep into the substrates owing to high residual stresses (Fig. 8A-iii). To terminate the cracks at the

Nanoscale Accepted Manuscript

predetermined positions, they fabricated stair-like multilevel micropatterns that can gradually release the propagation energy (Fig. 8A-iv). Subsequently, the concentrated tensile stress for crack propagation was fully relaxed at the multilevel terminating position, and the cracks were terminated successfully at the desired positions even under strong residual stresses. However, the propagation directions seem to be constrained to specific orientations because the cracks in the Si_3N_4 film penetrated deep into the crystallized Si substrate, resulting in limited multidirectional crack patterns or requiring additional steps for inserting an amorphous damper layer.

The effect of penetration depth on cracking in the Si_3N_4 film was addressed simply by changing the film material to SiO_2, which has lower residual stresses (Fig. 8B)[58]. Using a CVD-based cracking mechanism similar to that described above, *Alaca et al.* employed a sharp notch and open boundary trench to locally regulate the nominal tensile stress and control crack initiation and termination at predetermined positions. Stress-modulating microstructures were fabricated by RIE of the Si substrate to a 10 μm depth, and then a 5-μm-thick SiO_2 layer was deposited on top of the prefabricated Si wafer using PECVD. During annealing at 525 °C, crack patterns were generated from the sharp tip because of the residual tensile stress caused by condensation and volumetric shrinkage of the film. Because the residual stress of the SiO_2 film was much lower than that of the Si_3N_4 film[86], the cracks were localized only in the SiO_2 thin film without penetration into the Si substrate, resulting in perfect multidirectional crack patterns without any interference with the substrate (Fig. 8B). However, it seems difficult to obtain CVD-based crack patterns without multiple, complex fabrication processes, including Si etching and thin film deposition. Moreover, the crack patterns were quite susceptible to unwanted cracking because every sharp tip, including molecular level defects and impurities, may initiate cracks.

5.3. Crack-photolithography technique for constraint-free multidirectional cracks. Most recently, *Kim et al.* developed an innovative cracking-assisted nanofabrication method, so-called crack-photolithography, that can produce multidirectional and arbitrarily shaped crack patterns at

Nanoscale Accepted Manuscript

both the micro- and nanoscale using only the standard photolithography process (Fig. 9)[38]. First, a photomask with triangular and round microstructures was used for selectively UV-exposing a 10-μm-thick SU-8 film coated on a Si wafer. Then the SU-8 pattern was immersed in an SU-8 developer solution to simultaneously fabricate micropatterns and nanoscale crack patterns (Fig. 9A). To apply the necessary tensile stress for cracking during the development process, they produced crosslinking gradients in the SU-8 patterns along the normal direction to the substrate by simply eliminating the i-line UV filters. This novel process formed a relatively stiff SU-8 cluster (elastic layer) on top of a coarsely cured SU-8 underlayer (viscoelastic layer)[87], which enabled accurate crack control in the stiff top layer regulated by the underlayer creep[88, 89]. That is, the top and bottom layers consisted of a monolithic material with an inhomogeneous crosslinking density along the normal direction to the substrate. Consequently, an isotropic tensile stress was naturally applied during the development process for micropatterning, because the coarsely crosslinked underlayer expanded more than the top brittle layer owing to the mismatch in the swelling coefficients according to the crosslinking density[90]. This isotropic tensile stress was concentrated at the sharp tip points for crack initiation, and then the cracks were simultaneously propagated in every direction without bias toward a specific direction within the elastic layer (Fig. 9B). In addition, they adopted a double-photomask process to locally control the material properties of the SU-8, such as the fracture toughness, and perfectly prevented unwanted cracking even when sharp notches were present. Thus, crack patterns were selectively produced only in the single-exposure region because the double-exposure regions can be further strengthened by the second exposure[91]. Fig. 9C summarizes the controllability of the crack-photolithography technique: 1) no crack patterns were obtained using a round-round combination; 2) a straight crack pattern was obtained using a notch-round one; 3) a straight crack pattern was obtained by merging two counterpropagating cracks using a notch-notch one; and 4) no crack patterns appeared regardless of the microstructure shapes when the double-exposure process was used. By varying the crack control factors, *Kim et al.* fabricated

Nanoscale Accepted Manuscript

various mixed-scale micro/nanopatterns using the single- (Fig. 9D) or double-exposure process (Fig. 9E). For example, the Seoul metro map was replicated by crack patterns (nanopatterns) that were selectively produced only along the single-exposure regions to connect micropatterned metro stations.

Notably, crack photolithography enabled remarkable advances in crack control compared to previous crack lithography techniques. First, an isotropic, controllable tensile stress was spontaneously applied to an amorphous, homogeneous, and monolithic photoresist (e.g., SU-8) by swelling during the development process. This allowed comprehensive control of the crack directions and dimensions during crack crack-photolithography photolithography, which resulted in fabrication of well-organized, size-controllable, constraint-free, and multidirectional crack patterns. Second, the crack patterns were selectively produced only in predetermined single-exposure regions by blocking any unwanted cracks. In fact, unwanted crack generation was the biggest challenge and should be addressed to increase the production yield and reproducibility of previous crack lithography techniques. Crack-photolithography, however, fully resolved the critical issues by spatiotemporally adjusting the fracture toughness of the SU-8 film, thereby improving the quality and reliability of the micro/nanoscale crack patterns and their applications. Third, crack-photolithography requires no additional fabrication processes or equipment to produce nanoscale crack patterns over a large-scale wafer except for the standard microfabrication process (photolithography), and hence multiscale micro/nanopatterns can be easily fabricated in a cost- and time-effective manner.

6. Applications of the crack patterns

Crack lithography techniques have demonstrated their ability to produce micro/nanopatterns at high resolution over a large-scale substrate using facile fabrication procedures and simple, inexpensive facilities compared to conventional methods such as EBL, FIB lithography, and

Nanoscale Accepted Manuscript

MEMS-based techniques. In particular, cracking can open new surfaces having characteristics unlike those of the existing surfaces and/or increase the surface area in a confined volume, so there is high potential to use cracks for developing new functional materials and devices. In this section, we review recent advances in novel applications of crack lithography techniques in various research fields, including biological assays, micro/nanofluidic devices, nanowire-integrated devices, and sensory systems.

6.1. Cellular and biomolecular patterning platform. First of all, unidirectional crack lithography techniques based on thin film and elastomer systems can pattern cellular adhesive molecules (i.e., an extracellular matrix, ECM) by stretching and cracking a uniformly coated surfactant layer (Pluronic F108)[33]. Because the surfactant can prevent attachment of ECMs to a PDMS substrate, the unidirectional crack patterns allowed selective coating of ECMs by opening fresh and surfactant-free PDMS surfaces, which eventually enabled selective patterning of C2C12 myoblasts only along the ECM areas (Fig. 10A and B). In addition, the cellular morphology of the attached C2C12 cells was aligned along the crack patterns by repeated stretching and relaxation cycles of the strain because the cells can sense micro/nanoscale topographical features (Fig. 10C). Reconfigurable cellular patterning and manipulation were considered essential techniques to investigate cellular responses in dynamic environments during cell growth and differentiation. Typically, however, their use was limited by the complex fabrication steps required to prepare the selective cellular adhesive substrates. Therefore, micro/nanopatterns based on crack lithography seem to be quite effective for conducting rapid, low-cost biological assays because the crack patterns can be readily converted to micro/nanoscale cellular and/or biomolecular patterns over large areas (more than several centimeters squared) using simple procedures and inexpensive equipment. Given these advantages, crack-lithography-based bioassay platforms would provide scientists with significant insights into the fundamental relationships between cells and their environments, including cellular viability, proliferation, migration, and signal transduction[92, 93].

Nanoscale Accepted Manuscript

6.2. Integrated micro/nanofluidic device. Another important application of crack lithography is nanofluidic devices, the characteristic channel dimensions of which are comparable to those of small biomolecules and ions, including proteins and deoxyribonucleic acid (DNA). Typically, it has been challenging to integrate nanochannels with microfluidic devices on the same surface using conventional techniques because microfabrication and nanofabrication were performed in series with low compatibility (e.g., photolithography and EBL). For this reason, the multiscale micro/nanopatterns produced by crack lithography techniques have been highlighted as the most appropriate alternative for fabricating integrated micro/nanofluidic devices. Here, we introduce two types of integrated micro/nanofluidic devices that were developed using different crack lithography techniques.

First, *Huh et al.* generated unidirectional nanoscale crack patterns on an oxidized PDMS substrate and integrated the patterns with another PDMS layer having microchannels[36]. The oxide layer on the PDMS substrate was stretched sufficiently to produce many unidirectional cracks that were perpendicularly aligned with the applied tensile strain, which is essentially the procedure explained in Fig. 10. Then the nanoscale crack patterns were replicated using a UV-curable epoxy that was again used as a master for soft lithography to fabricate PDMS-based nanochannels. After the soft lithography, the PDMS nanopatterns were bonded with another microfabricated PDMS layer (microchannels) to form a liquid-tight, size-tunable micro/nanochannel network to be applied for linearization (stretching) of coiled DNA. Although they established a new paradigm for fabricating integrated micro/nanofluidic devices using crack lithography, it seems to be difficult to accurately control the nanochannel position and number owing to the lack of stress-modulating microstructures. In addition, the nanochannels and microchannels were prepared separately in different PDMS layers, so additional alignment steps were essential. Moreover, there seem to be potential compatibility issues with complex micro/nanofluidic channel designs.

Nanoscale Accepted Manuscript

Second, recently *Kim and Kim* developed an advanced technique for fabricating integrated micro/nanofluidic devices by adopting crack photolithography, which can simultaneously generate multiscale micro/nanopatterns on the same surface (Fig. 11)[59]. Because the micropatterns and nanopatterns (cracks) were fabricated on the same surface using a single photolithography process, they can be automatically aligned and integrated from the early design stage (Fig. 11A). In addition, the dimensions, position, and number of the cracks were accurately controlled by employing stress-modulating microstructures and adjusting the process parameters of crack photolithography (Fig. 11B), which enabled manipulation of the transport of small molecules in microchannels at will (Fig. 11C). Therefore, a microfluidic channel network can be facilely integrated with nanochannel arrays that can function as diffusion-controlling but convection-suppressing nanostructures in microfluidic devices with highly robust, accurate, and expandable diffusion control. As an application of such micro/nanofluidic devices, they characterized the cell-to-cell communication of synthetic bacterial cells and found that the cells can chemically communicate with each other by extracellular diffusive microenvironments that were completely engineered using the nanochannel array (Fig. 11D). Hence, crack photolithography would facilitate the development of unprecedented micro/nanofluidic devices for a wide range of nanofluidic and biological applications.

6.3. Nanowire-integrated gas sensor. Crack lithography was also widely used to fabricate nanowire-integrated devices to detect and monitor gaseous environments[94, 95]. One-dimensional nanowires have generally been intensively studied because of their ultrahigh surface-area-to-volume ratio, which enables detection of a few gas molecules with a faster response time, lower power consumption, and greater portability than conventional sensors based on 2-D thin films[96]. However, current fabrication approaches still rely on conventional bottom-up[97, 98] or top-down[99, 100] techniques. Therefore, crack lithography techniques for nanoscale patterning have high potential to replace the current top-down or bottom-up approaches because they not only produce multiscale

Nanoscale Accepted Manuscript

micro/nanopatterns on the same surface but also accurately control the dimensions and directions of the nanowires up to a few tens of nanometers[35, 38].

For instance, *Jebril et al.* fabricated a bow-tie-like micropattern in a photoresist film on a Si wafer to create a nanoscale crack pattern in the middle, weakest point of the photoresist by thermal cycling to induce a tensile stress[42, 94, 95]. As shown in Fig. 12A and B, the nanocrack micropattern served as a masking structure during deposition of a metallic nanowire material (zinc oxide, ZnO) by sputtering, followed by a lift-off process to remove excess metal on the photoresist mask. Because the micropatterns and nanowires (cracks) were produced on the same surface, the nanowires were automatically aligned and connected to microelectrodes for signal transduction (Fig. 12C). The ZnO nanowires were used to detect oxygen (O_2) gas at partial pressures from 0.2 to 1000 mbar. Under UV illumination, the O_2 gas was changed to reactive O_2 species such as O^{2-}, O_2^-, and O^-, which were easily adsorbed into the ZnO nanowire surface to form O_2 vacancies in the nanowires even at room temperature[101]. Thus, the resistivity of the nanowires can be sensitively and selectively changed according to the O_2 partial pressure[95, 101, 102]. Increasing the O_2 partial pressure decreased the current passing through the nanowires, as shown in Fig. 12D. The principal sensor characteristics, such as the sensitivity, selectivity, and dynamic range, were superior to those of a control nanowire-integrated device fabricated by a conventional expensive nanofabrication technique (EBL)[94]. Therefore, the crack lithography technique made it successful to fabricate nanowire-integrated microchips in a high-throughput and facile manner by batch processing. Because the produced gas sensors enabled quantitative detection of a few gas molecules, crack lithography techniques could be applied to fabricate other types of nanowires[95] by using various substrates, including flexible films[103, 104].

6.4. Multi-functional mechanosensor. Increasing attention has been given to the development of multifunctional mechanosensors that can detect human motions, including moving, typing, talking, breathing, and even the heart beating by being attached to the skin or clothes[105, 106].

Nanoscale Accepted Manuscript

However, it has been difficult for state-of-the-art vibration/strain sensors based on thin films to fully satisfy the technical demands such as ultrahigh mechanosensitivity with both high flexibility and high durability in repeated bending and/or stretching cycles. Recently, *Kang et al.* reported crack-lithography-based multifunctional mechanosensors inspired by the spider sensory system (Fig. 13A)[39]. The mechanosensors used reversible disconnection and reconnection processes based on zip-like nanoscale crack junctions that can transduce small mechanical changes (i.e., strain) into large electrical signals (i.e., resistivity). To fabricate the nanoscale crack sensor, a platinum (Pt) thin layer was deposited on a flexible polyurethane acrylate (PUA) layer on a polyethylene terephthalate (PET) film by sputtering. Both the PUA and PET polymers were flexible enough to bend or stretch without cracking, but the brittle Pt layer cracked under even a small tensile stain, so a number of unidirectional crack patterns formed in the metallic layer (Fig. 13B).

Similar to the case of cracks in a brittle film on an elastomeric substrate presented above, the crack density and dimensions were controlled by varying the bending radius of curvature, which determines the applied tensile stress. After the crack patterns were created, the nanoscale crack sensor was connected to metal electrodes to transduce the resistivity changes into current signals during motion detection. Interestingly, the nanoscale crack sensor was unprecedentedly sensitive to axial elongation and compression, because the resistivity of the cracked film was dramatically increased or decreased according to disconnection or reconnection events at the cracked surfaces. Thus, the sensitivity of the nanoscale crack sensor was highly enhanced by the disconnection-reconnection events, whereas the metallic film without crack patterns, which is the same as that in conventional strain gages, was not as sensitive as the nanoscale crack sensor owing to the absence of disconnection-reconnection events. The nanoscale crack sensor, which had a radius of curvature of 1 mm during crack generation, exhibited 450-fold higher sensitivity than the normal sensor without crack patterns at 0.5% strain. Furthermore, the nanoscale crack sensor showed high reproducibility and durability even for 5,000 cyclic fatigue tests because the brittle film was already

Nanoscale Accepted Manuscript

cracked, and the other polymeric layers were quite flexible; an inflexible and uncracked sensor is typically susceptible to fatigue cracks.

As an application of mechanosensors based on nanoscale cracks, a 5 cm × 5 cm sensing network consisting of 8 × 8 arrays, the individual sensing units of which are 2 mm × 2 mm in size, was fabricated and attached to a violin for real-time monitoring of sound waves. As shown in Fig. 13C, the mechanosensors accurately distinguished the vibration from the G, D, A, and E strings, which showed different vibrational amplitudes and frequencies. Based on the calibration of the basic sound waves, the sensor successfully converted the mechanical vibration during a performance of Elgar's *Salut d'Amour* into digital signals by time sequential and *in situ* monitoring of the sound waves. Additionally, *Kang et al.* demonstrated that multifunctional crack sensors can detect various mechanical signals from a small insect, speech patterns, and even heartbeat rates (Fig. 13D). Therefore, crack lithography has high potential for application to various mechanosensors or piezo-resistive actuators, including health-care devices, thin film actuators, and real-time environmental monitoring devices with high mechanosensitivity, controllability, and durability[107].

Conclusions

Over the last few decades, a number of experimental and theoretical approaches have been attempted to understand and manipulate nanoscale cracks in order to produce well-defined small patterns with greatly reduced cost and time consumption compared to conventional nanofabrication. To provide a brief overview of the developmental history of crack lithography techniques, Table 1 summarizes representative crack lithography techniques and their features. Notably, the crack patterns depend strongly on the cracking mechanism, stress source, material properties of the thin films and substrates, and fabrication process and equipment. In addition, it is important to control the dimensions and directionality of cracks during their initiation, propagation, and termination. Consequently, these factors determine applications of the cracks.

Nanoscale Accepted Manuscript

Initially, most research focused on investigation of cracking phenomena occurring in various microfabrication processes to identify the underlying fundamentals of nanoscale cracks. *Skjeltorp and Meakin* observed randomly oriented cracks in a self-assembled polystyrene monolayer and found that cracking arose from volume shrinkage of individual polystyrene spheres during a continuous drying process[67]. Such drying-mediated random cracks were widely used for producing functional surfaces or enhancing surface characteristics because they can create new surface areas[68].

Huh et al. and other researchers applied uniaxial strain/stress to impose a directional alignment on the randomly oriented cracks[36]. The strain-controlled cracks were fabricated by simple uniaxial stretching or bending without expensive micro/nanofabrication equipment. In addition, unidirectional cracks can produce a number of nanoscale straight lines with controllable density and dimensions. Thus, the crack patterns were used for biological patterning platforms, nanofluidic devices, nanowire-integrated devices, and even multifunctional mechanosensors. However, control of the axial strain or stress was limited to a few directions, and hence various mechanisms for applying isotropic stresses were developed to further increase the directional controllability.

Next, *Nam et al.* and other researchers used the residual film stress generated in various CVD processes, including those of widely used dielectric thin films such as SiO_2 and Si_3N_4[35]. The residual film stress, which is isotropic and homogeneous, was induced by the mismatch in thermal expansion between the thin films and substrates, and the nominal stress was locally concentrated or released by stress-modulating microstructures. That is, stress modulators such as notches and open boundaries played an important role in initiating and terminating cracks at predetermined positions. Furthermore, multidirectional crack patterns were fabricated by batch fabrication so that a number of nanopatterns (cracks) can be simultaneously created over a large-scale wafer, enabling high-throughput, cost-efficient nanofabrication. However, the cracking process involves expensive

Nanoscale Accepted Manuscript

equipment and multiple complex fabrication processes, including photolithography, SiO_2/Si_3N_4 CVD, RIE, and even DRIE. Moreover, the directional freedom can be limited by the substrate constraints when the cracks in the thin films penetrated deep into a substrate having a crystallographic orientation.

Subsequently, to overcome these limitations, a constraint-free, single-photolithography-based cracking mechanism was developed by *Kim et al*[38]. In particular, the stress was applied using spontaneous isotropic swelling phenomena during photoresist development; therefore, no additional nanofabrication processes were required, except for the standard microfabrication (photolithography) process. In addition, the crack dimensions and pathways were completely engineered by adjusting the UV exposure energy, the intensity of which can be spatiotemporally controlled using additional photomasks with a resolution of several microns. Therefore, constraint-free multidirectional crack patterns with locally controllable dimensions and directions can be facilely produced throughout a large-scale wafer. Owing to the high crack controllability, multidirectional crack patterns can cover all possible applications of unidirectional cracks with increased patterning directions and density.

In conclusion, state-of-the-art crack lithography techniques enabled us to fabricate nanoscale patterns with both high resolution and high throughput, which have been difficult to achieve simultaneously using conventional nanofabrication techniques. In particular, crack lithography techniques have accelerated the use of nanotechnology in individual laboratories even where expensive facilities and particular fabrication skills were unavailable, resulting in the development of novel and specific applications. However, further efforts should be made to expand the applicable materials, because the cracking mechanism seems to differ substantially, depending on the specifications of the material (i.e., for ceramics, metals, polymers, and elastomers). In addition, downsizing the nanoscale cracks toward single-molecule-level disassembly will open new opportunities not only for the development of advanced metamaterials and novel nanodevices but

Nanoscale Accepted Manuscript

also for use as an accurate experimental platform to study the fundamental physics and mechanics of material fractures in the near future.

ACKNOWLEDGEMENTS

This work was supported by the National Research Foundation of Korea (NRF) grant funded by the Korea government (MSIP) (NRF-2014R1A2A1A10050431).

Nanoscale Accepted Manuscript

References

1. C. D. O'Connell, M. J. Higgins, S. E. Moulton and G. G. Wallace, *J Mater Chem C*, 2015, **3**, 6431-6444.
2. S. S. Yao and Y. Zhu, *Adv Mater*, 2015, **27**, 1480-1511.
3. K. Kim, J. Guo, X. Xu and D. L. Fan, *Small*, 2015, **11**, 4037–4057.
4. B. Z. Tian, X. L. Zheng, T. J. Kempa, Y. Fang, N. F. Yu, G. H. Yu, J. L. Huang and C. M. Lieber, *Nature*, 2007, **449**, 885-889.
5. A. Rinaldi, P. Peralta, C. Friesen, D. Nahar, S. Licoccia, E. Traversa and K. Sieradzki, *Small*, 2010, **6**, 528-536.
6. M. Schvartzman, M. Palma, J. Sable, J. Abramson, X. A. Hu, M. P. Sheetz and S. J. Wind, *Nano Lett*, 2011, **11**, 1306-1312.
7. L. M. Dai, D. W. Chang, J. B. Baek and W. Lu, *Small*, 2012, **8**, 1130-1166.
8. Z. Y. Wang and Z. H. Dai, *Nanoscale*, 2015, **7**, 6420-6431.
9. M. Altissimo, *Biomicrofluidics*, 2010, **4**, 026503.
10. A. A. Tseng, K. Chen, C. D. Chen and K. J. Ma, *Ieee T Electron Pack*, 2003, **26**, 141-149.
11. H. He, J. C. She, Y. F. Huang, S. Z. Deng and N. S. Xu, *Nanoscale*, 2012, **4**, 2101-2108.
12. R. Thakar, A. E. Weber, C. A. Morris and L. A. Baker, *Analyst*, 2013, **138**, 5973-5982.
13. Z. M. Han, M. Vehkamaki, M. Leskela and M. Ritala, *Nanotechnology*, 2014, **25**, 115302.
14. J. Kim, Y. U. Lee, B. Kang, J. H. Woo, E. Y. Choi, E. S. Kim, M. Gwon, D. W. Kim and J. W. Wu, *Nanotechnology*, 2013, **24**, 015306.
15. P. D. Yang, Z. J. Zhang, J. T. Hu and C. M. Lieber, *Mater Res Soc Symp P*, 1997, **438**, 593-598.
16. C. L. Shen, Y. Peng, K. H. Wang and Q. Zhou, *Radiat Phys Chem*, 2013, **83**, 8-14.
17. V. R. Manfrinato, L. H. Zhang, D. Su, H. G. Duan, R. G. Hobbs, E. A. Stach and K. K. Berggren, *Nano Lett*, 2013, **13**, 1555-1558.
18. L. J. Guo, *Adv Mater*, 2007, **19**, 495-513.
19. C. Peroz, S. Dhuey, M. Cornet, M. Vogler, D. Olynick and S. Cabrini, *Nanotechnology*, 2012, **23**, 015305.
20. L. J. Guo, *J Phys D Appl Phys*, 2004, **37**, R123-R141.
21. P. D. Yang, G. Wirnsberger, H. C. Huang, S. R. Cordero, M. D. McGehee, B. Scott, T. Deng, G. M. Whitesides, B. F. Chmelka, S. K. Buratto and G. D. Stucky, *Science*, 2000, **287**, 465-467.
22. Y. C. Wang and J. Y. Han, *Lab Chip*, 2008, **8**, 392-394.

Nanoscale Accepted Manuscript

23. C. H. Duan and A. Majumdar, *Nat Nanotechnol*, 2010, **5**, 848-852.

24. R. Karnik, R. Fan, M. Yue, D. Y. Li, P. D. Yang and A. Majumdar, *Nano Lett*, 2005, **5**, 943-948.

25. H. J. Zeng, Z. L. Wang and A. D. Feinerman, *Nanotechnology*, 2006, **17**, 3183-3188.

26. A. Pimpin and W. Srituravanich, *Eng. J.*, 2011, 37−55.

27. J. Haneveld, H. Jansen, E. Berenschot, N. Tas and M. Elwenspoek, *J Micromech Microeng*, 2003, **13**, S62-S66.

28. C. H. Duan, W. Wang and Q. Xie, *Biomicrofluidics*, 2013, **7**, 026501.

29. P. Mao and J. Y. Han, *Lab Chip*, 2005, **5**, 837-844.

30. M. B. Stern, M. W. Geis and J. E. Curtin, *J Vac Sci Technol B*, 1997, **15**, 2887-2891.

31. D. J. Green, R. Tandon and V. M. Sglavo, *Science*, 1999, **283**, 1295-1297.

32. K. T. Leung, L. Jozsa, M. Ravasz and Z. Neda, *Nature*, 2001, **410**, 166-166.

33. X. Y. Zhu, K. L. Mills, P. R. Peters, J. H. Bahng, E. H. Liu, J. Shim, K. Naruse, M. E. Csete, M. D. Thouless and S. Takayama, *Nat Mater*, 2005, **4**, 403-406.

34. M. P. Rao, A. J. Sanchez-Herencia, G. E. Beltz, R. M. McMeeking and F. F. Lange, *Science*, 1999, **286**, 102-105.

35. K. H. Nam, I. H. Park and S. H. Ko, *Nature*, 2012, **485**, 221-224.

36. D. Huh, K. L. Mills, X. Y. Zhu, M. A. Burns, M. D. Thouless and S. Takayama, *Nat Mater*, 2007, **6**, 424-428.

37. A. Yuse and M. Sano, *Nature*, 1993, **362**, 329-331.

38. M. Kim, D. Ha and T. Kim, *Nat Commun*, 2015, **6**, 6247.

39. D. Kang, P. V. Pikhitsa, Y. W. Choi, C. Lee, S. S. Shin, L. F. Piao, B. Park, K. Y. Suh, T. I. Kim and M. Choi, *Nature*, 2014, **516**, 222-226.

40. B. E. Alaca, C. Ozcan and G. Anlas, *Nanotechnology*, 2010, **21**, 055301.

41. O. Sardan, A. D. Yalcinkaya and B. E. Alaca, *Nanotechnology*, 2006, **17**, 2227-2233.

42. R. Adelung, O. C. Aktas, J. Franc, A. Biswas, R. Kunz, M. Elbahri, J. Kanzow, U. Schurmann and F. Faupel, *Nat Mater*, 2004, **3**, 375-379.

43. B. C. Kim, T. Matsuoka, C. Moraes, J. X. Huang, M. D. Thouless and S. Takayama, *Sci Rep*, 2013, **3**, 3027.

44. B. C. Kim, C. Moraes, J. X. Huang, T. Matsuoka, M. D. Thouless and S. Takayama, *Small*, 2014, **10**, 4020-4029.

45. J. Marthelot, B. Roman, J. Bico, J. Teisseire, D. Dalmas and F. Melo, *Phys Rev Lett*, 2014, **113**, 085502.

Nanoscale Accepted Manuscript

46. A. Nakahara and Y. Matsuo, *Phys Rev E*, 2006, **74**, 045102.

47. W. H. Koo, S. M. Jeong, F. Araoka, K. Ishikawa, S. Nishimura, T. Toyooka and H. Takezoe, *Nat Photonics*, 2010, **4**, 222-226.

48. N. Bowden, S. Brittain, A. G. Evans, J. W. Hutchinson and G. M. Whitesides, *Nature*, 1998, **393**, 146-149.

49. H. Q. Jiang, D. Y. Khang, J. Z. Song, Y. G. Sun, Y. G. Huang and J. A. Rogers, *Proc Natl Acad Sci USA*, 2007, **104**, 15607-15612.

50. C. M. Stafford, C. Harrison, K. L. Beers, A. Karim, E. J. Amis, M. R. Vanlandingham, H. C. Kim, W. Volksen, R. D. Miller and E. E. Simonyi, *Nat Mater*, 2004, **3**, 545-550.

51. X. Chen and J. Yin, *Soft Matter*, 2010, **6**, 5667-5680.

52. S. Chung, J. H. Lee, M. W. Moon, J. Han and R. D. Kamm, *Adv Mater*, 2008, **20**, 3011-3016.

53. K. Efimenko, M. Rackaitis, E. Manias, A. Vaziri, L. Mahadevan and J. Genzer, *Nat Mater*, 2005, **4**, 293-297.

54. P. Kim, M. Abkarian and H. A. Stone, *Nat Mater*, 2011, **10**, 952-957.

55. J. B. Kim, P. Kim, N. C. Pegard, S. J. Oh, C. R. Kagan, J. W. Fleischer, H. A. Stone and Y. L. Loo, *Nat Photonics*, 2012, **6**, 327-332.

56. B. Li, Y. P. Cao, X. Q. Feng and H. J. Gao, *Soft Matter*, 2012, **8**, 5728-5745.

57. E. B. Gorokhov, V. Y. Prinz, A. G. Noskov and T. A. Gavrilova, *J Electrochem Soc*, 1998, **145**, 2120-2131.

58. B. E. Alaca, H. Sehitoglu and T. Saif, *Appl Phys Lett*, 2004, **84**, 4669-4671.

59. M. Kim and T. Kim, *Anal Chem*, 2015, **87**, 11215–11223.

60. R. Chantiwas, S. Park, S. A. Soper, B. C. Kim, S. Takayama, V. Sunkara, H. Hwang and Y. K. Cho, *Chem Soc Rev*, 2011, **40**, 3677-3702.

61. B. C. Kim, C. Moraes, J. X. Huang, M. D. Thouless and S. Takayama, *Biomater Sci*, 2014, **2**, 288-296.

62. D. M. Robertson, D. Robertson and C. R. Barrett, *J Biomech*, 1978, **11**, 359-364.

63. T. Khatun, T. Dutta and S. Tarafdar, *Appl Clay Sci*, 2013, **86**, 125-128.

64. M. Mirkhalaf, A. K. Dastjerdi and F. Barthelat, *Nat Commun*, 2014, **5**, 3166.

65. R. Khandelwal and J. M. C. Kishen, *Int J Solids Struct*, 2008, **45**, 6157-6176.

66. N. Vandenberghe, R. Vermorel and E. Villermaux, *Phys Rev Lett*, 2013, **110**, 174302.

67. A. T. Skjeltorp and P. Meakin, *Nature*, 1988, **335**, 424-426.

68. K. D. M. Rao, R. Gupta and G. U. Kulkarni, *Adv Mater Interfaces*, 2014, **1**, 1400090.

Nanoscale Accepted Manuscript

69. J. C. Li, X. Gong, D. Wang and D. C. Ba, *Appl Phys a-Mater*, 2013, **111**, 645-651.

70. K. Luke, A. Dutt, C. B. Poitras and M. Lipson, *Opt Express*, 2013, **21**, 22829-22833.

71. G. C. Hill, J. I. Padovani, J. C. Doll, B. W. Chui, D. Rugar, H. J. Mamin, N. Harjee and B. L. Pruitt, *J Micromech Microeng*, 2011, **21**, 087001.

72. S. Mani and T. M. Saif, *Appl Phys Lett*, 2005, **86**, 201903.

73. S. Mani and T. Saif, *Thin Solid Films*, 2007, **515**, 3120-3125.

74. O. Sardan, B. E. Alaca, A. D. Yalcinkaya, P. Boggild, P. T. Tang and O. Hansen, *Nanotechnology*, 2007, **18**, 375501.

75. X. H. Liu, Z. Suo, Q. Ma and H. Fujimoto, *Eng Fract Mech*, 2000, **66**, 387-402.

76. A. C. Orifici, P. Wongwichit and N. Wiwatanawongsa, *Compos Part a-Appl S*, 2014, **66**, 218-226.

77. X. Zhang, K. S. Chen and S. M. Spearing, *Sensor Actuat a-Phys*, 2003, **103**, 263-270.

78. Z. C. Xia and J. W. Hutchinson, *J Mech Phys Solids*, 2000, **48**, 1107-1131.

79. D. Salac and W. Lu, *Comp Mater Sci*, 2007, **39**, 849-856.

80. J. X. Huang, B. C. Kim, S. Takayama and M. D. Thouless, *J Mater Sci*, 2014, **49**, 255-268.

81. K. L. Mills, X. Y. Zhu, S. C. Takayama and M. D. Thouless, *J Mater Res*, 2008, **23**, 37-48.

82. H. Vandeparre, Q. H. Liu, I. R. Minev, Z. G. Suo and S. P. Lacour, *Adv Mater*, 2013, **25**, 3117-3121.

83. Q. Zhuang, S. C. Warren, B. Baytekin, A. F. Demirors, P. P. Pillai, B. Kowalczyk, H. T. Baytekin and B. Grzybowski, *Adv Mater*, 2014, **26**, 3667-3672.

84. H. Schmid and B. Michel, *Macromolecules*, 2000, **33**, 3042-3049.

85. T. W. Odom, J. C. Love, D. B. Wolfe, K. E. Paul and G. M. Whitesides, *Langmuir*, 2002, **18**, 5314-5320.

86. O. Zohni, G. Buckner, T. Kim, A. Kingon, J. Maranchi and R. Siergiej, *J Micromech Microeng*, 2007, **17**, 1042-1051.

87. M. Jamal, A. M. Zarafshar and D. H. Gracias, *Nat Commun*, 2011, **2**, 527.

88. J. Liang, R. Huang, J. H. Prevost and Z. Suo, *Exp Mech*, 2003, **43**, 269-279.

89. R. Huang, J. H. Prevost and Z. Suo, *Acta Mater*, 2002, **50**, 4137-4148.

90. Z. Zhou, Q. A. Huang, W. H. Li, W. Lu, Z. Zhu and M. Feng, *Ieee Sensor*, 2007, 10.1109/Icsens.2007.4388402, 325-328.

91. S. Keller, G. Blagoi, M. Lillemose, D. Haefliger and A. Boisen, *J Micromech Microeng*, 2008, **18**, 125020.

Nanoscale Accepted Manuscript

92. C. S. Chen, M. Mrksich, S. Huang, G. M. Whitesides and D. E. Ingber, *Science*, 1997, **276**, 1425-1428.

93. M. Thery, A. Jimenez-Dalmaroni, V. Racine, M. Bornens and F. Julicher, *Nature*, 2007, **447**, 493-496.

94. S. Jebril, M. Elbahri, G. Titazu, K. Subannajui, S. Essa, F. Niebelschutz, C. C. Rohlig, V. Cimalla, O. Ambacher, B. Schmidt, D. Kabiraj, D. Avasti and R. Adelung, *Small*, 2008, **4**, 2214-2221.

95. D. Gedamu, S. Jebril, A. Schuchardt, M. Elbahri, S. Wille, Y. K. Mishra and R. Adelung, *Phys Status Solidi B*, 2010, **247**, 2571-2580.

96. F. Patolsky, G. Zheng and C. M. Lieber, *Nanomedicine*, 2006, **1**, 51-65.

97. A. Nerowski, J. Opitz, L. Baraban and G. Cuniberti, *Nano Res*, 2013, **6**, 303-311.

98. C. O'Dwyer, M. Szachowicz, G. Visimberga, V. Lavayen, S. B. Newcomb and C. M. S. Torres, *Nat Nanotechnol*, 2009, **4**, 239-244.

99. Y. G. Sun, R. A. Graff, M. S. Strano and J. A. Rogers, *Small*, 2005, **1**, 1052-1057.

100. X. Yu, Y. C. Wang, H. Zhou, Y. X. Liu, Y. Wang, T. Li and Y. L. Wang, *Small*, 2013, **9**, 525-530.

101. N. M. Kiasari and P. Servati, *Ieee Electr Device L*, 2011, **32**, 982-984.

102. M. Takata, D. Tsubone and H. Yanagida, *J Am Ceram Soc*, 1976, **59**, 4-8.

103. A. R. Madaria, A. Kumar, F. N. Ishikawa and C. W. Zhou, *Nano Res*, 2010, **3**, 564-573.

104. C. H. Liu and X. Yu, *Nanoscale Res Lett*, 2011, **6**, 75.

105. S. P. Sane, A. Dieudonne, M. A. Willis and T. L. Daniel, *Science*, 2007, **315**, 863-866.

106. D. Son, J. Lee, S. Qiao, R. Ghaffari, J. Kim, J. E. Lee, C. Song, S. J. Kim, D. J. Lee, S. W. Jun, S. Yang, M. Park, J. Shin, K. Do, M. Lee, K. Kang, C. S. Hwang, N. S. Lu, T. Hyeon and D. H. Kim, *Nat Nanotechnol*, 2014, **9**, 397-404.

107. M. Kaltenbrunner, T. Sekitani, J. Reeder, T. Yokota, K. Kuribara, T. Tokuhara, M. Drack, R. Schwodiauer, I. Graz, S. Bauer-Gogonea, S. Bauer and T. Someya, *Nature*, 2013, **499**, 458-463.

Nanoscale Accepted Manuscript

Figures and Table

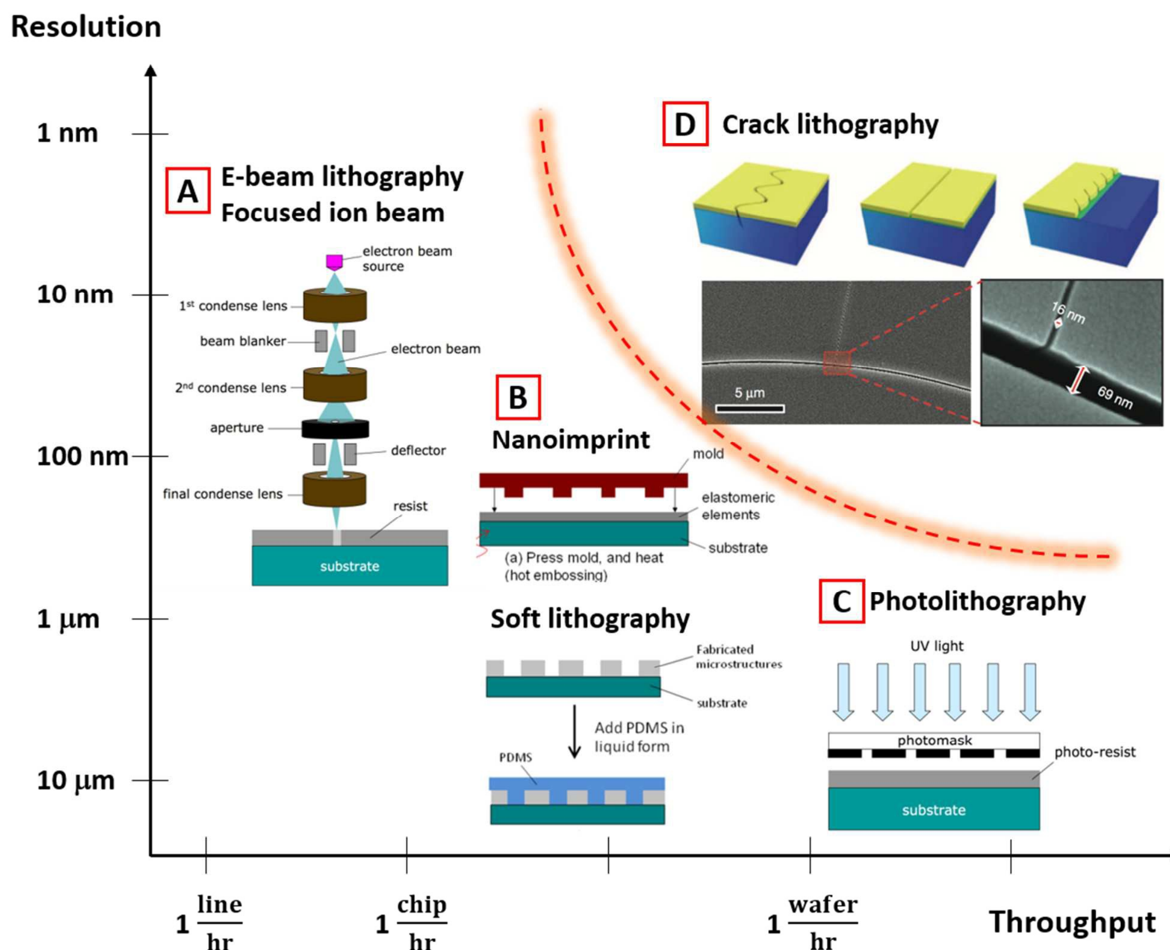

Figure 1. Overview of conventional nanofabrication and unconventional crack lithography techniques. (A) Conventional nanolithography techniques such as EBL and FIB lithography show high patterning resolution, but the throughput is limited because these are direct writing methods. Reproduced with permission[26]. (B) Replica molding techniques such as nanoimprint and soft lithography exhibit intermediate levels of both resolution and throughput. Reproduced with permission[26]. (C) Photolithography exhibits high throughput because of batch processing, but the minimum feature sizes are usually limited to a few microns. Reproduced with permission[26]. (D) Crack lithography, a new nanopatterning concept using intentional cracking, generates nanopatterns over a large-scale film on a substrate. Theoretically, it can produce patterns at the single-molecule level over an entire material simultaneously, resulting in both high resolution and high throughput. Reproduced with permission[35].

Nanoscale Accepted Manuscript

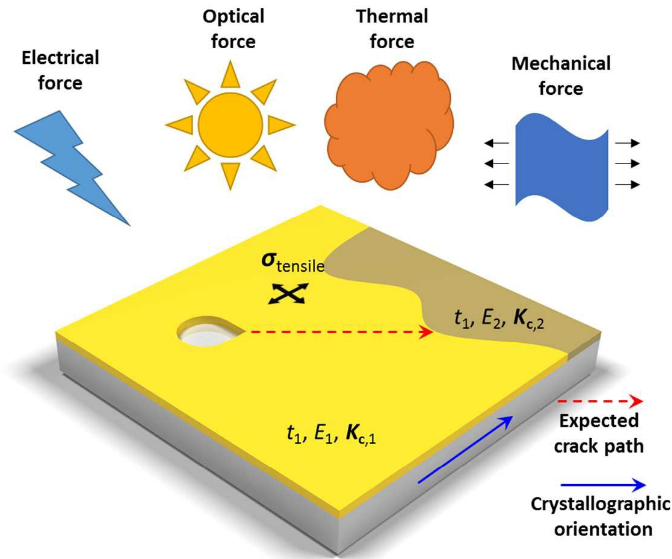

Figure 2. Schematic showing a crack in a thin film on a substrate due to a tensile stress field ($\boldsymbol{\sigma}_{\mathrm{tensile}}$). An external force such as an electrical, optical, thermal, or mechanical force can apply tensile stress. The film has two regions with different material properties, for example, the film thickness (t_1, t_2), Young's modulus (E_1, E_2), and fracture toughness ($\boldsymbol{K}_{\mathrm{c},1}$, $\boldsymbol{K}_{\mathrm{c},2}$). In addition, the crack in the thin film on the substrate will be affected by the crystallographic orientation of the substrate.

Nanoscale Accepted Manuscript

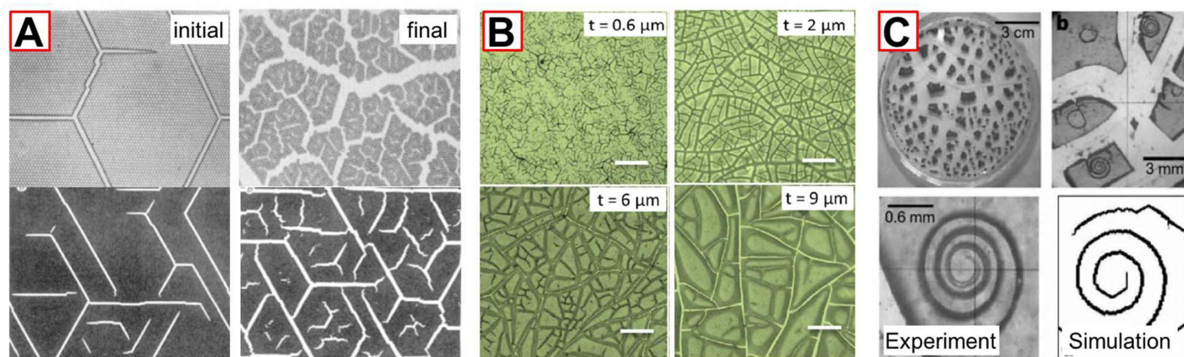

Figure 3. Drying-mediated, randomly oriented crack patterns. (A) Straight linear cracks in a self-assembled polystyrene monolayer developed into fractal-like chaotic crack patterns during a continuous drying process. Top and bottom images show experimental and simulation results, respectively. Reproduced with permission[67]. (B) Drying-mediated cracks showed different cracking dimensions and densities according to the film thickness, which ranged from 0.6 to 9 μm. Reproduced with permission[68]. (C) Crack pattern with a spiral profile was observed in a dried nickel phosphate precipitate. Reproduced with permission[32].

Nanoscale Accepted Manuscript

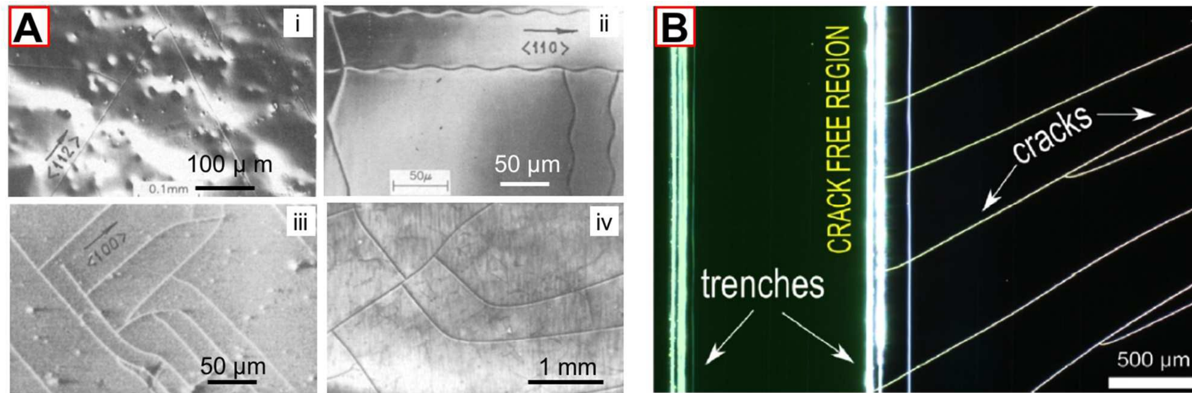

Figure 4. Randomly oriented crack patterns observed in various CVD processes. (A) Crack patterns depended strongly on the CVD parameters: i) crack patterns in a SiO_2 film on the (111)-oriented CdHgTe substrate, ii) crack patterns in a Si_3N_4 film on the (100)-oriented Si substrate, iii) crack patterns in the (001)-oriented Si substrate after a Si_3N_4 film was removed, and iv) constraint-free crack patterns in a SiO_2 film on the (111)-oriented Ge substrate with a GeO_2 interlayered film as a damping structure. Reproduced with permission[57]. (B) Propagating cracks in a Si_3N_4 thin film, which also penetrated deep into the Si substrate, terminated at the crack-free region (trenches). Reproduced with permission[70].

Nanoscale Accepted Manuscript

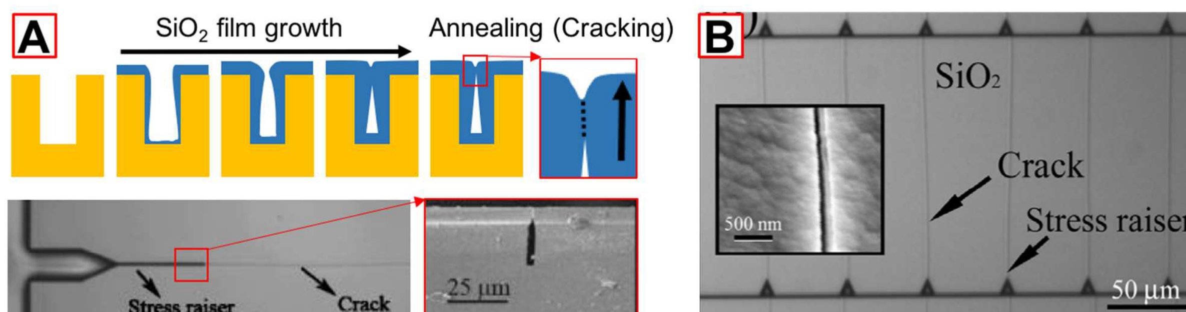

Figure 5. CVD-based unidirectional crack patterns. (A) Schematic diagram showing a straight crack that was guided by a sharp triangular void structure (stress raiser) formed inside the SiO_2 film. Stress-concentrating void structures were fabricated using a deep micropatterned trench on a Si wafer, which induced non-conformal deposition. Bottom pictures are top and cross-sectional SEM images. Reproduced with permission[72]. (B) Unidirectional crack arrays in a SiO_2 film were initiated at triangular notch structures (stress raisers) and terminated at the line patterns (stress releasers). Inset shows a magnified SEM image of the crack pattern. Reproduced with permission[40].

Nanoscale Accepted Manuscript

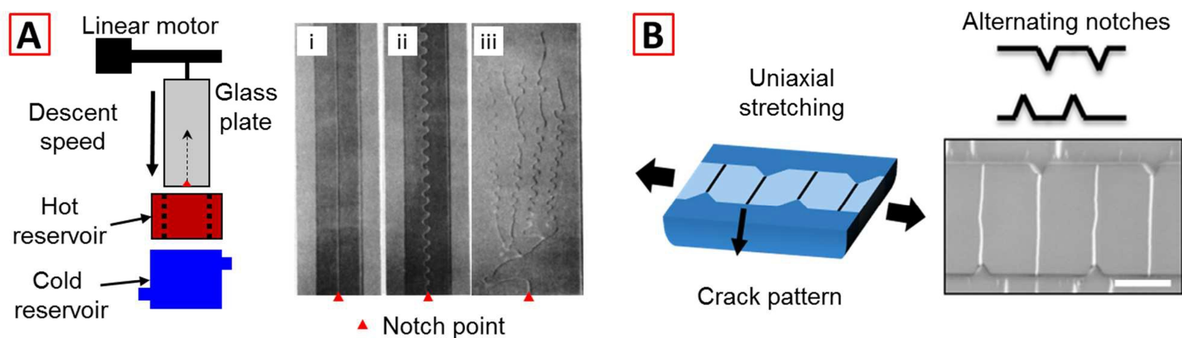

Figure 6. Unidirectional crack patterns obtained by controlling axial stresses or strains. (A) Various unidirectional crack patterns, such as i) linear, ii) oscillating, and iii) nonlinear profiles, were induced on glass substrates (sample size 24 × 64 × 0.13 mm^3) by uniaxial thermal stress. The uniaxial thermal stress was controlled by varying the temperature differences between hot and cold reservoirs with different descent speeds (quenching rates). Reproduced with permission[37]. (B) Strain-controlled unidirectional crack patterns fabricated in a brittle thin film (i.e., metal or oxidized PDMS layer) on an elastomer substrate (PDMS). Alternating notch pairs showed a high production yield for creating linear cracks. Reproduced with permission[43].

Nanoscale Accepted Manuscript

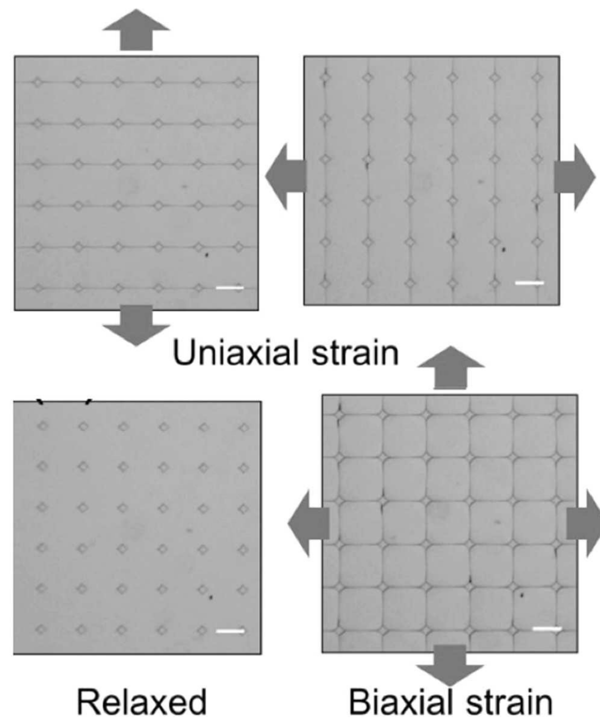

Figure 7. Strain-controlled bidirectional crack patterns. Biaxial strain created microscale crack patterns in an h-PDMS layer on a PDMS substrate, guided by diamond-shaped notch structures for local stress concentration. Microscale cracks were recovered to nanoscale crack patterns by eliminating the biaxial strain. Reproduced with permission[44].

Nanoscale Accepted Manuscript

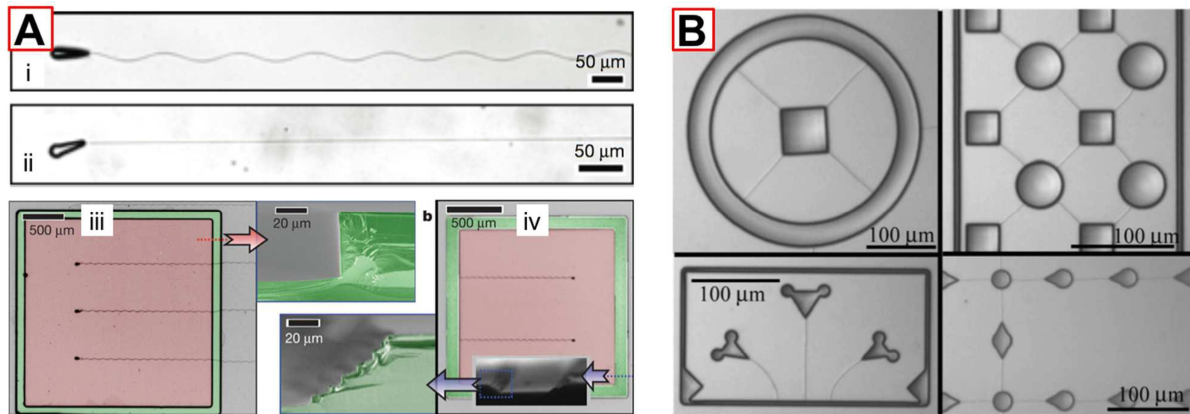

Figure 8. CVD-based multidirectional crack patterns. (A) Microscopic images show crack propagation and termination in a Si_3N_4 film. Cracks in the Si_3N_4 film penetrated deep into the Si substrate, resulting in i) oscillating (without the SiO_2 interlayer) or ii) linear (with the SiO_2 interlayer) crack patterns. Propagating cracks were difficult to terminate (iii) at the simple trench structure because of crack penetration into the substrate, but they were successfully terminated (iv) at the multilevel stair-like microstructures. Interestingly, the crack patterns in the Si_3N_4 film were multidirectional, but the directional freedom can be constrained by adjusting the crystallographic orientation of the Si substrate. Reproduced with permission[35]. (B) Various multidirectional crack patterns created in a SiO_2 layer on a prefabricated Si substrate. Notched microstructures in the Si wafer controlled the crack patterns. Notably, the cracks in the SiO_2 thin films did not penetrate the substrate, showing constraint-free multidirectional crack patterns. Reproduced with permission[58].

Nanoscale Accepted Manuscript

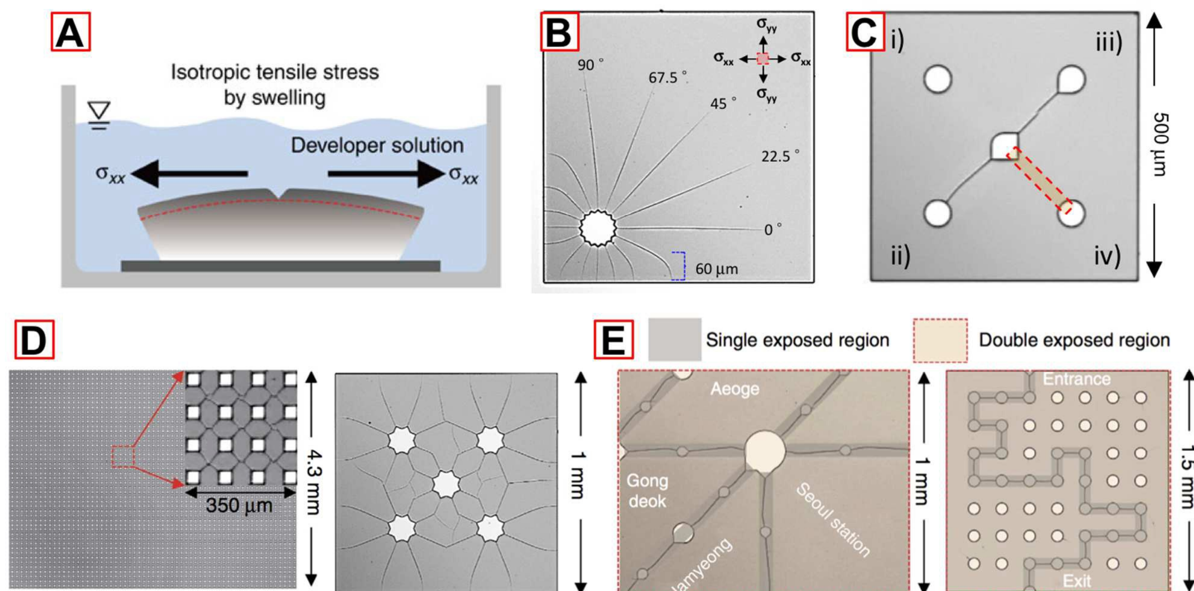

Figure 9. Constraint-free multidirectional crack patterns during photolithography-based microfabrication. (A) Isotropic and controllable tensile stress was spontaneously applied during development of the photoresist (SU-8). (B) Isotropic nature of the tensile stress and SU-8 films enabled generation of perfect multidirectional crack patterns. (C) The crack photolithography technique controlled not only the local stress fields but also the local material strength by using additional photomasks, as shown in the four cracking cases (i, ii, iii, and iv). Various multidirectional crack patterns were produced by the (D) single- or (E) double-photomask process. Notably, crack patterns were localized in the single-exposure region, but no unwanted cracks were generated in the double-exposure region even when sharp tips were present. Reproduced with permission[38].

Nanoscale Accepted Manuscript

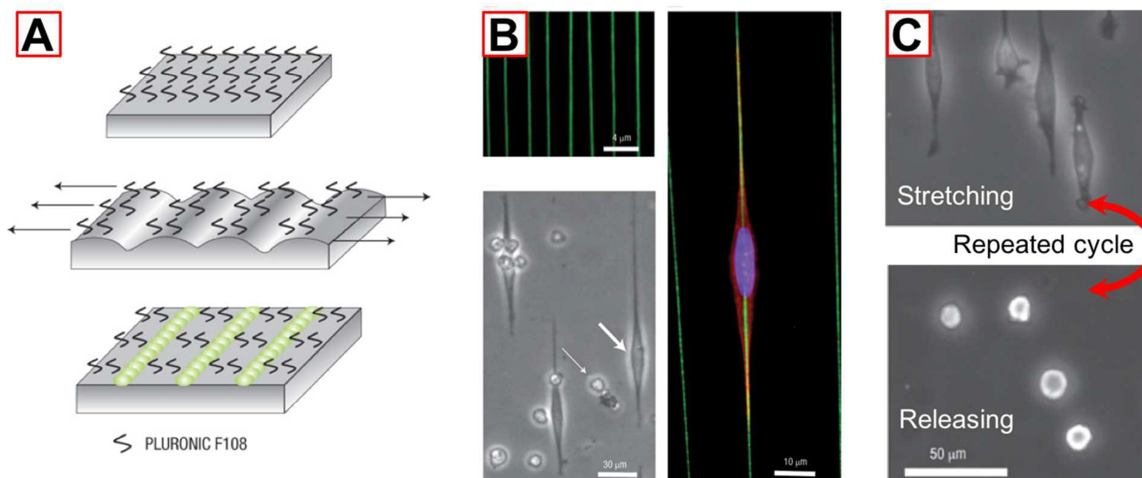

Figure 10. Application of crack patterns for biomolecular/cellular patterning and analysis. (A) Surfactant layer (Pluronic F108) was uniformly coated on a PDMS substrate, followed by stretching (cracking) process to create a surfactant-free PDMS surface for selective coating with cellular adhesive molecules. (B) Microscopic images show the patterned fluorescent biomolecules and C2C12 myoblast cells. (C) Repeated stretch and release cycles were periodically applied to characterize morphological features of the cells in a dynamic cellular environment. Reproduced with permission[33].

Nanoscale Accepted Manuscript

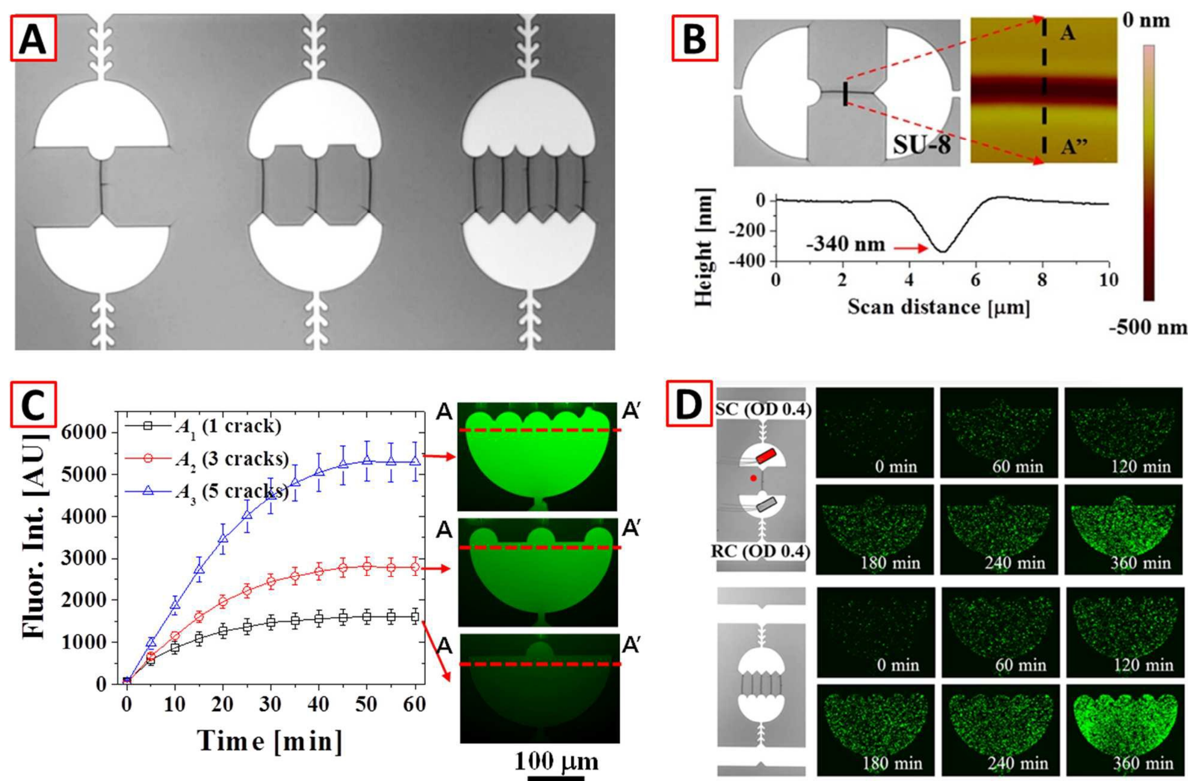

Figure 11. Integrated micro/nanofluidic devices for controlling diffusion transport of biomolecules. (A) Microscopic image showing SU-8 micropatterns and nanoscale crack arrays fabricated on the same surface. (B) Microscopy and atomic force microscopy images showing the crack dimensions, which are nanoscale in height but microscale in width. (C) Diffusion rate of a fluorescent molecule was linearly controlled according to the nanochannel (crack) numbers. (D) Diffusion-controlled micro/nanofluidic device enabled characterization of the genetic induction and cell-to-cell signaling of synthetically engineered bacterial cells. Notably, the expression of the green fluorescent protein was accurately engineered by varying the length and number of nanochannels. Reproduced with permission[59].

Nanoscale Accepted Manuscript

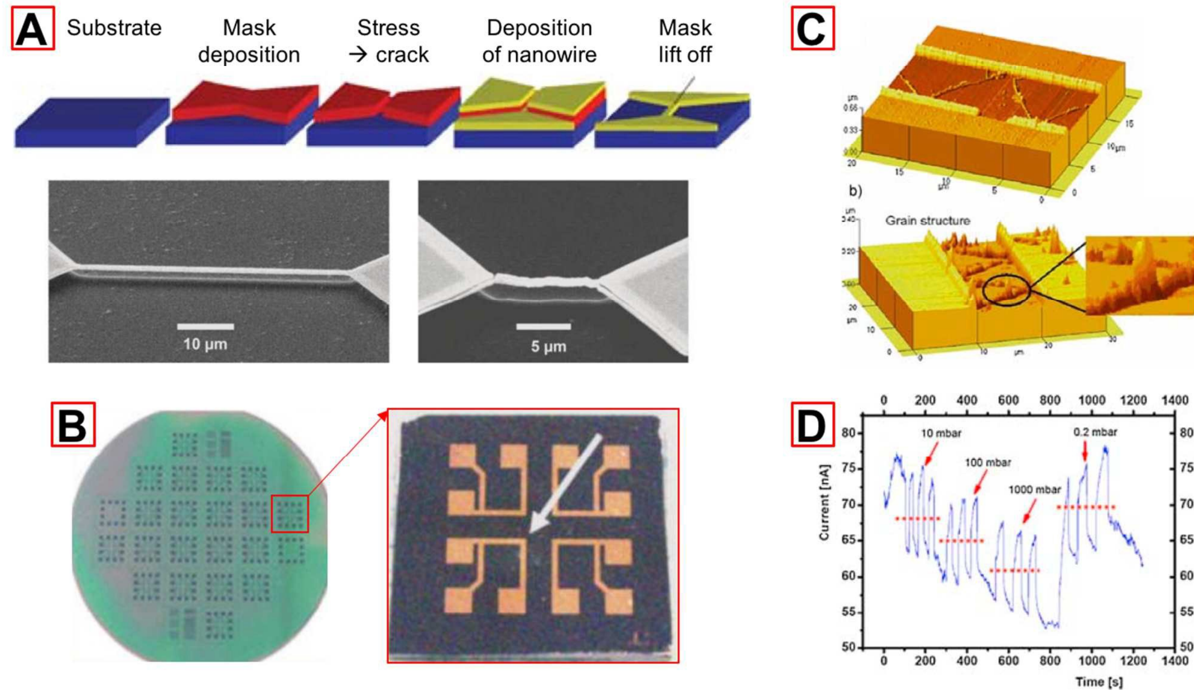

Figure 12. Nanowire-integrated microchips for detecting gas molecules. (A) Schematic showing fabrication procedures for the nanowires using crack lithography. SEM images at the bottom show a fabricated metal nanowire that connects micropatterned metal pads. (B) Multiple nanowire-integrated devices on a wafer scale obtained using batch fabrication by crack lithography. (C) Atomic force microscopy images showing zigzag oriented Ti nanowires between two micropatterns. (D) Current signals detected by ZnO nanowires under different partial pressures of O_2 gas. Reproduced with permission[94, 95].

Nanoscale Accepted Manuscript

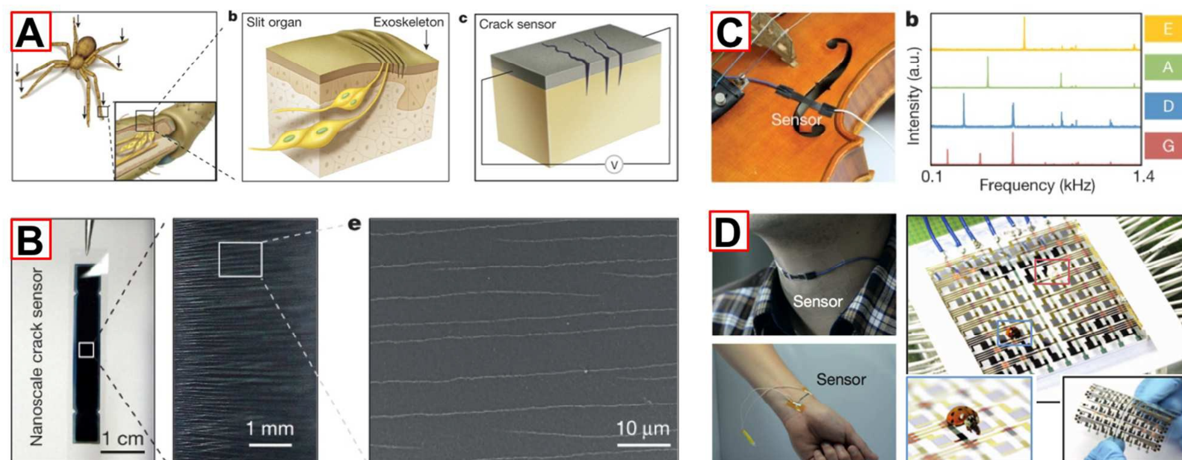

Figure 13. Multifunctional nanocrack-based mechanosensors inspired by the spider. (A) Schematic showing the similarity between the spider's sensory system and the nanocrack sensors. (B) Nanocracks were fabricated by bending Pt thin films on a PUA substrate attached to a PET film. Inset SEM image shows a number of unidirectional nanoscale cracks produced in the Pt layer. (C) Nanocrack sensor was attached to the curved surface of a violin to measure sound waves from the violin strings. (D) Nanocrack sensor detected various mechanical signals such as pressure and vibration signals while attached to human skin or curved surfaces because of its flexibility. Reproduced with permission[39].

Nanoscale Accepted Manuscript

Table 1. Summary of representative crack lithography techniques

Ref.	Drying-mediated cracks[67]	Strain-controlled cracks[36]	CVD-based cracks[35]	Photolithography-based cracks[38]
Crack patterns	Randomly oriented	Unidirectional	Constrained multidirectional	Constraint-free multidirectional
Generation mechanism	Volume shrinkage of wetted particle during drying process	Mismatch of elastic modulus between thin film and substrate layer	Mismatch of thermal expansion between thin film and substrate layers	Mismatch of swelling volume in differently cross-linked photoresist
Material	Polystyrene monolayer on Si substrate	Oxide film on PDMS substrate	Si_3N_4 film on Si substrate	SU-8 film on Si substrate
Stress source	Drying (isotropic tensile stress)	Mechanical stretching (uniaxial tensile stress)	Residual film stress (isotropic tensile stress)	Swelling (isotropic tensile stress)
Crack initiation	Global control (random position)	Global control (random position)	Local control (notched position)	Local control (notched position)
Crack propagation	Random (depending on the drying condition)	Anisotropic depending on the direction of applied uniaxial stress	Anisotropic depending on crystallographic orientation of substrate	Isotropic without dependency on substrate
Crack termination	Uncontrollable	Uncontrollable	Spatial control (stair-like microstructure)	Spatiotemporal control (exposure energy and development time)
Dimension of crack	W = several microns H = several microns (uncontrollable)	W = 500–2000 nm H = ~ 100 nm (globally controllable by strain rate)	W = ~ 100 nm H = ~ 1000 nm (uncontrollable)	W = 300–3000 nm H = 30–300 nm (locally controllable by exposure energy)
Fabrication process	1) Monolayer coating 2) Drying process	1) Preparation of PDMS slab 2) Oxide layer deposition 3) Applying mechanical stress	1) Photolithography 2) SiO_2 deposition 3) SiO_2 reactive ion etching (RIE) 4) Si Deep-RIE 5) Si_3N_4 deposition	1) Photolithography
Required equipment	Desiccator	Mask aligner, O_2 plasma, stretching jig	Mask aligner, RIE-etcher, DRIE etcher, LPCVD	Mask aligner
Application	Functional surface, sensor	Functional surface, nanofluidic device, nanowire, sensor, actuator		

Nanoscale Accepted Manuscript